Article

Neuron

Graded Control of Climbing-Fiber-Mediated Plasticity and Learning by Inhibition in the Cerebellum

Highlights

- Purkinje cell dendritic spiking is suppressed respective to MLI activity levels
- Increasing inhibition converts LTD into LTP along a continuous spectrum
- MLI activation alters the magnitude and valence of motor learning
- Graded climbing fiber Ca^{2+} signaling by MLIs expands error coding in the cerebellum

Authors

Matthew J.M. Rowan, Audrey Bonnan, Ke Zhang, ..., Hiroki Taniguchi, George J. Augustine, Jason M. Christie

Correspondence

jason.christie@mpfi.org

In Brief

By linking inhibitory control of Purkinje cell dendritic Ca^{2+} signaling to alteration of plasticity and learning, Rowan et al. provide a mechanistic framework by which MLIs influence the ability of climbing fibers to instruct adaptive behavior in the cerebellum.

Rowan et al., 2018, Neuron *99*, 999–1015
September 5, 2018
https://doi.org/10.1016/j.neuron.2018.07.024

CellPress

Neuron
Article

Graded Control of Climbing-Fiber-Mediated Plasticity and Learning by Inhibition in the Cerebellum

Matthew J.M. Rowan,[1,6] Audrey Bonnan,[1,6] Ke Zhang,[1,2,3,6] Samantha B. Amat,[1] Chikako Kikuchi,[1] Hiroki Taniguchi,[1] George J. Augustine,[4,5] and Jason M. Christie[1,7,*]
[1]Max Planck Florida Institute for Neuroscience, Jupiter, FL, USA
[2]Integrative Biology and Neuroscience Graduate Program, Florida Atlantic University, Jupiter, FL, USA
[3]International Max Planck Research School for Brain and Behavior, Florida Atlantic University, Jupiter, FL, USA
[4]Lee Kong Chian School of Medicine, Nanyang Technological University, Singapore, Singapore
[5]Institute of Molecular and Cell Biology, Singapore, Singapore
[6]These authors contributed equally
[7]Lead Contact
*Correspondence: jason.christie@mpfi.org
https://doi.org/10.1016/j.neuron.2018.07.024

SUMMARY

Purkinje cell dendrites convert excitatory climbing fiber input into signals that instruct plasticity and motor learning. Modulation of instructive signaling may increase the range in which learning is encoded, yet the mechanisms that allow for this are poorly understood. We found that optogenetic activation of molecular layer interneurons (MLIs) that inhibit Purkinje cells suppressed climbing-fiber-evoked dendritic Ca^{2+} spiking. Inhibitory suppression of Ca^{2+} spiking depended on the level of MLI activation and influenced the induction of associative synaptic plasticity, converting climbing-fiber-mediated potentiation of parallel fiber-evoked responses into depression. In awake mice, optogenetic activation of floccular climbing fibers in association with head rotation produced an adaptive increase in the vestibulo-ocular reflex (VOR). However, when climbing fibers were co-activated with MLIs, adaptation occurred in the opposite direction, decreasing the VOR. Thus, MLIs can direct a continuous spectrum of plasticity and learning through their influence on Purkinje cell dendritic Ca^{2+} signaling.

INTRODUCTION

Adaptive behavior relies on neural mechanisms that support the flexibility necessary for a multitude of different outcomes. In the cerebellum, a brain region that plays a prominent role in motor learning, adaptive behaviors result from motor errors that trigger learning. While the exact mechanism through which motor learning occurs is unknown, its basis must depend on instructive signals that guide plasticity (Carey et al., 2005; Ito, 1972; Medina et al., 2002; Schultz and Dickinson, 2000). Operating under a simple algorithm, a learning rule could be set so that an instructive signal relays the necessity for one type of learning in a simple, binary manner: either learning is to occur or it should not. However, such a constraint may be too rigid to encode the continuum of learning necessary for complex motor behavior (Boyden et al., 2004). This dilemma may be avoided by providing instruction in a regulated or multiplexed manner.

Climbing fibers (CFs) projecting from the inferior olive (IO) to the cerebellar cortex produce instructive signals that mediate learning. Within the cerebellar cortex, CFs make powerful excitatory connections onto Purkinje cells (PCs) that evoke somatic complex spikes and widespread, regenerative dendritic Ca^{2+} action potentials (Davie et al., 2008; Otsu et al., 2014; Rancz and Häusser, 2006). The resulting elevation of dendritic Ca^{2+} concentration provides a biochemical trigger for inducing synaptic plasticity at co-active parallel fiber (PF) inputs. This includes long-term depression (LTD), a form of synaptic weakening induced by the associative activity of CFs (Finch et al., 2012; Linden and Connor, 1995). The reliability of CFs in eliciting complex spikes and plasticity led to the notion that instruction produced by their activity occurs in an invariant or ''all-or-none'' manner (Eccles et al., 1966). However, an emerging view indicates that the PC response to CF excitation in awake animals is subject to regulation and is graded depending on behavioral context (Kimpo et al., 2014; Najafi and Medina, 2013; Yang and Lisberger, 2014). A key circuit element that may contribute to the regulation of the CF response is the inhibitory activity of molecular layer interneurons (MLIs) (Callaway et al., 1995). Through GABA release onto the somata and dendrites of postsynaptic PCs, MLIs modulate simple spike output and dendritic excitability through feedforward and lateral inhibition (Dizon and Khodakhah, 2011; Häusser and Clark, 1997; Mittmann et al., 2005). Yet the consequences of MLI inhibition on CF-evoked excitation, plasticity, and learning are poorly understood.

In this study, we used optogenetics to precisely activate MLIs and systematically examine their influence on CF-mediated

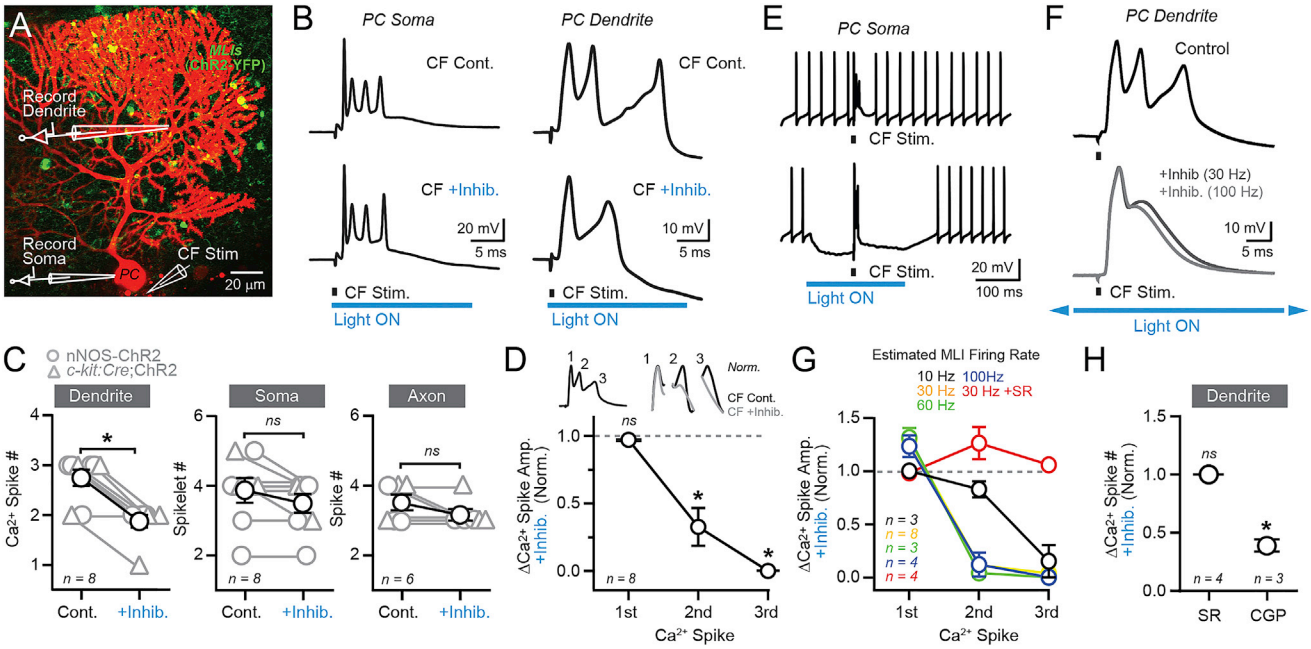

Figure 1. MLIs Suppress CF-Evoked Dendritic Ca^{2+} Spiking in PCs

(A) A dye-filled PC imaged with 2pLSM; MLIs expressing YFP-tagged ChR2 are in green.

(B) Spiking responses in the soma and dendrite of a PC to CF stimulation, both in control and during coincident optogenetic activation of MLIs (timing of light stimulus in blue; electrical stimulus in black).

(C) The subcellular effect of optogenetic-induced MLI inhibition on CF-evoked spiking content in the dendrite (84.6 ± 11.6 µm from the axon hillock; range, 38.1–140.6 µm), soma, and axon (97.8 ± 36.4 µm from the axon hillock; range, 21.0–178.0 µm). Measurements from individual cells are in gray, average in black. *p = 0.0002; paired t test.

(D) The change in amplitude of dendritic Ca^{2+} spikes during optogenetic excitation of MLIs. Data are normalized to control responses for each spike in the burst recorded in the absence of optogenetic stimulation (indicated by the gray dotted line in the plot). Example traces of spikes are shown above. *p < 0.05; one-way ANOVA with Dunnett's post-test.

(E) Example traces of CF-evoked complex spikes, both in control and during persistent optogenetic excitation of MLIs.

(F) CF-evoked dendritic Ca^{2+} spikes recorded in PCs during different levels of MLI activity (top trace is in the absence of MLI activity). The firing rate of MLIs during the optogenetic stimulus was an estimate based on a separate set of calibration experiments.

(G) Changes in Ca^{2+} spike amplitude depended on the level of MLI activation. Data from individual cells are normalized to control responses for each spike as indicated by the gray dotted line (see Table S1 for statistics).

(H) Across-cell comparison of the effect of MLI inhibition on dendritic Ca^{2+} spike content in the presence of SR 95531 or CPG 35348. Data are normalized to control trials without optogenetic-induced inhibition. *p = 0.04; paired t tests.

All data are mean ± SEM. See also Figures S1–S3.

instructive signaling. Our quantitative measurements from PCs in acute cerebellar slices indicate that inhibition from MLIs suppresses CF-evoked dendritic Ca^{2+} spiking in an activity-dependent manner. Through graded control of dendritic Ca^{2+} elevation, MLI activity progressively overrides the ability of CFs to elicit associative synaptic plasticity that weakens PF-evoked potentials. Instead, the increasing contribution of MLIs to the integrated CF-evoked dendritic response results in strengthening of PF-mediated excitation. *In vivo*, control of synaptic plasticity by MLIs was reflected in learned motor responses encoded in the vestibulo-cerebellum. Pairing optogenetic activation of CFs with head rotation produced an increase in vestibulo-ocular reflex (VOR) gain. In contrast, when we co-activated CFs and MLIs using dual-color optogenetics, there was a learned decrease in VOR gain. Together, our findings point to a key role for MLIs in regulating plasticity and learning in the cerebellum.

RESULTS

MLI-Mediated Suppression of Dendritic Ca^{2+} Spiking in PCs

To evaluate the subcellular influence of MLI-mediated inhibition on CF-evoked excitation, we made multisite whole-cell recordings from PCs in acute cerebellar slices from nNOS-ChR2 mice under near-physiological conditions (Figure 1A; STAR Methods). Electrical stimulation of CFs (1 Hz) elicited complex spikes in PC somata and large-amplitude excitatory postsynaptic potentials (EPSPs) with superimposed bursts of Ca^{2+} spikes in their dendrites (Davie et al., 2008; Figure 1B). Because nNOS-ChR2 mice express ChR2 exclusively in nearly all MLIs (Kim et al., 2014; Figure S1A), we used optogenetics to evoke MLI-mediated inhibition. Wide-field illumination with a brief pulse of blue light (λ = 461 nm; 20 ms; 2.4 mW/mm^2) recruited an MLI ensemble that approximates the coherent population activity of

MLIs observed during motor behavior (Gaffield and Christie, 2017). Activating MLIs coincident with CF-evoked excitation of PCs diminished the number of Ca^{2+} spikes in the dendritic burst and substantially reduced spike amplitude subsequent to the initial response (Figures 1B–1D). Similar results were obtained using *c-kit::Cre* mice (Amat et al., 2017) expressing ChR2 in MLIs via Cre-dependent adeno-associated virus (AAV) transduction (Figure 1C). Therefore, these mice were used interchangeably with nNOS-ChR2 animals in our experiments. The brief MLI stimulus had no effect on spikelet content during the complex spike in the soma (Figures 1B and 1C). Likewise, the conversion of CF excitation into action potential output, measured using subcellular-targeted patching of the axon past the point of spike initiation, was unaffected by coincident activation of MLIs (Figures 1C, S2A, and S2B). The subcellular specificity of MLI activity on the dendritic response is likely due to the fact that CF excitation is compartmentalized in PCs, such that Ca^{2+} spikes are generated independently in the dendrite, and burst firing in the axon manifests as spikelets in the somatic complex spike waveform (Davie et al., 2008; Otsu et al., 2014).

Mechanisms of PC Dendritic Spike Suppression by Inhibition under Physiological Conditions

During motor behavior, MLIs spike in a sustained manner; their activity encodes the kinematic features of movements (Chen et al., 2017; Gaffield and Christie, 2017; Jelitai et al., 2016). Thus, we next wanted to determine the extent to which MLI activity effectively suppresses PC dendritic Ca^{2+} spiking under these conditions. To approximate this physiological context, we elicited persistent firing in ChR2-expressing MLIs across a behaviorally relevant range of spiking frequencies (10–100 Hz; Jelitai et al., 2016; Ozden et al., 2012; ten Brinke et al., 2015). In this approach, a separate set of recordings from ChR2-expressing MLIs was used to estimate the relationship between photostimulus intensity and the average firing rate of activated cells (Figure S1B). Using these pre-calibrated light powers to drive varying levels of MLI activity, CFs were stimulated well after the onset of MLI firing (Figure 1E), thereby avoiding the initial epoch of highly synchronous, optogenetic-induced output. We observed a graded influence of inhibition on somatic complex spikes with different intensities of MLI stimulation. This included a reduction in both burst duration and spikelet content, reflecting diminished action potential output in the axon (Figures S3A and S3B). Therefore, inhibition can modulate CF-evoked action potential output in PCs under conditions that recruit dense and sustained activity of MLIs. Dendritic Ca^{2+} spiking was also suppressed by persistent MLI stimuli, yielding graded reductions in spike amplitude that saturated with modest levels of MLI activity (Figures 1F and 1G). Ca^{2+} spike suppression by persistent MLI activity was also apparent when CFs were stimulated less frequently (0.1 Hz); this condition produces stronger CF excitatory drive onto PCs due to diminished synaptic depression (Dittman and Regehr, 1998; Hashimoto and Kano, 1998; Figure S3C). These results indicate that MLI-mediated inhibition can suppress PC dendritic spiking across a wide range of physiological conditions.

Bath application of the selective $GABA_A$ receptor antagonist SR 95531 (20 μM) blocked the ability of sustained MLI activity to suppress CF-evoked dendritic spiking (Figures 1G and 1H). In contrast, dendritic spike suppression was insensitive to the $GABA_B$ receptor antagonist CGP 35348 (20 μM; Figure 1H). This indicates that MLIs modulate dendritic spike activity through a rapid, electrogenic effect on the postsynaptic PC. The suppressive effect of MLI activity on Ca^{2+} spikes could be mimicked by hyperpolarizing the cell by somato-dendritic current injection (−17.9 mV from a holding potential of −57.7 mV; Figure S3D), consistent with the known sensitivity of dendritic spikes to membrane potential (Kitamura and Häusser, 2011; Otsu et al., 2014; Wang et al., 2000). From a hyperpolarized potential, there was no influence of MLI excitation on the CF-evoked response (Figure S3D). Together, these results show that, through $GABA_A$ receptor-mediated inhibition, MLIs increase the apparent signaling range of CFs beyond all-or-none excitation by generating graded suppression of dendritic Ca^{2+} spiking and axonal action potential output.

MLI-Mediated Suppression of CF-Evoked Intracellular Ca^{2+} Elevation

CF-evoked dendritic spiking increases the concentration of intracellular Ca^{2+}, a ubiquitous biochemical messenger in signal transduction pathways. To directly examine the modulatory effect of MLIs on CF-evoked Ca^{2+} signals, PCs were loaded with a low-affinity green Ca^{2+} indicator (Fluo-5F), and their dendritic shafts were imaged with 2-photon laser-scanning microscopy (2pLSM) (Figure 2A). During imaging, MLIs were activated with amber light using the red-shifted opsin bReaChES (Rajasethupathy et al., 2015; λ = 596 nm; 20 ms; 0.47 mW/mm^2). Compared to ChR2, use of bReaChES improved the chromatic compatibility of optogenetic photostimulation and functional imaging incorporating green-light-emitting Ca^{2+} fluorophores. When CF excitation of PCs coincided with optogenetic activation of MLIs, the resulting dendritic Ca^{2+} transients were reduced in amplitude (61.3% ± 3.2% of control; n = 12; p = 0.0004; paired t test; Figure 2B). We assessed the relationship between MLI activity and the suppression of CF-evoked dendritic Ca^{2+} elevation using pre-calibrated photostimulus intensities. With this approach, we could predictably vary MLI activity to match that produced by ChR2 excitation (Figure S1C), thus facilitating comparisons across conditions. MLI-induced suppression of CF-evoked dendritic Ca^{2+} transients occurred in a graded manner and increased with the intensity of MLI activation (Figures 2C and 2D).

CF-evoked Ca^{2+} signals in PC spines are enhanced when CFs are stimulated in conjunction with PFs (Finch et al., 2012; Wang et al., 2000). This non-linearity is thought to reflect a PF-induced change in dendrite excitability that facilitates Ca^{2+} spike propagation into spiny branchlets, yielding additional Ca^{2+} entry into dendrites (Otsu et al., 2014). To determine whether CF-evoked Ca^{2+} signals remain sensitive to MLI-mediated inhibition following conjunctive PF activity, we paired a brief PF tetanus with CF stimulation and measured the resulting Ca^{2+} signals in the spines of distal PC branchlets (Figure 2E). The Ca^{2+} response to conjunctive stimulation of these two inputs (peak amplitude = ΔF/F 37.5 ± 6.1) was greater than the expected linear sum of their individual components (expected peak amplitude from sum of CF and PF alone = ΔF/F 28.4 ± 3.9; n = 21 spines; p = 0.002;

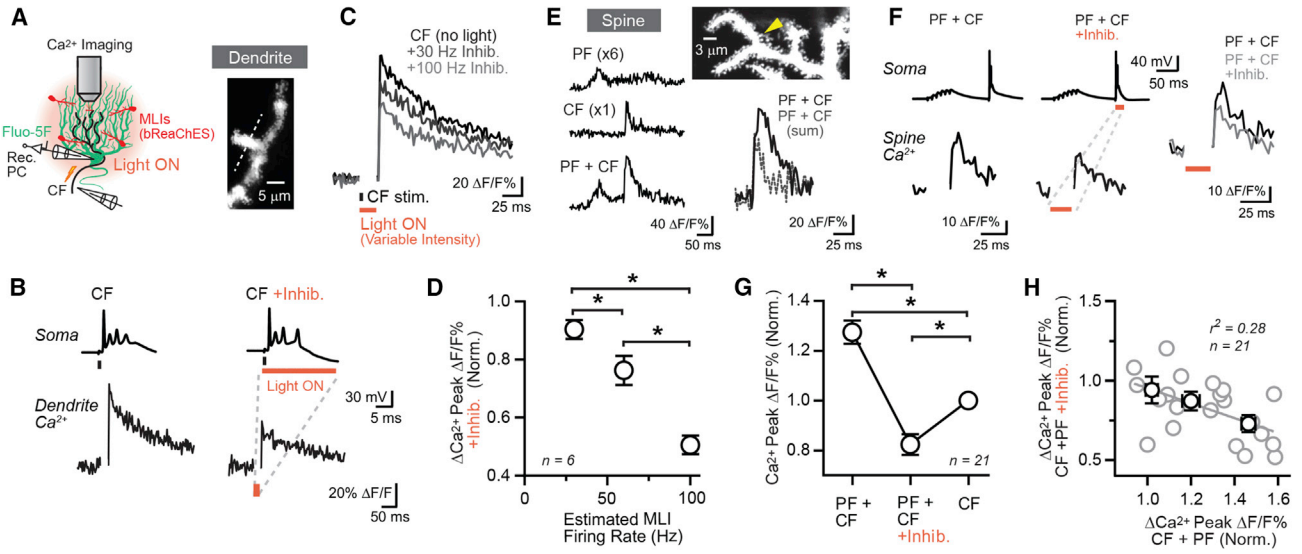

Figure 2. Graded Suppression of CF-Evoked Dendritic Ca^{2+} Signals in PCs by MLI-Mediated Inhibition

(A) 2pLSM Ca^{2+} imaging was performed in the dendrites of PCs. MLIs in *c-kit::Cre* mice were transduced by AAV containing Cre-dependent bReaChES. The position of the line scan used to record the CF-evoked Ca^{2+} response is demarcated by the dotted line in the dendrite image.

(B) CF-evoked somatic complex spikes (top traces) and dendritic Ca^{2+} transients (bottom traces) in control (left) and during optogenetic stimulation of MLIs (right; timing of light stimulus in orange; electrical stimulus in black).

(C) Dendritic Ca^{2+} transients measured in PCs during different levels of MLI excitation.

(D) Relationship between the suppression of dendritic Ca^{2+} elevation and the level of MLI excitation. Measurements from many different dendritic recording sites were collected from three PCs. *$p < 0.05$; repeated-measures one-way ANOVA with Tukey's post-test.

(E) Average Ca^{2+} transients measured from the spine demarcated by the yellow arrowhead in the fluorescence image in response to a PF tetanus (100 Hz; 60 ms), CF stimulation, or the conjunctive activation of both (120 ms inter-stimulus interval). On the right, magnified view of the CF-evoked Ca^{2+} transient following conjunctive PF activity in comparison to the estimated response from the linear sum of the individual PF and CF transients.

(F) CF-evoked Ca^{2+} transients measured in a PC spine following conjunctive activation with PFs (left) and with coincident MLI-mediated inhibition (middle). Response in control and during bReaChES-induced MLI excitation coincident with the CF stimulus is superimposed (right).

(G) Effect of optogenetic-induced MLI inhibition on the peak CF-evoked Ca^{2+} transient during conjunctive stimulation with PFs. Responses, collected from spine measurements from six PCs, were normalized to the peak amplitude of the Ca^{2+} transient elicited by CF stimulation alone for each recording site. *$p < 0.05$; repeated-measures one-way ANOVA with Tukey's post-test.

(H) Relationship between the PF enhancement of CF Ca^{2+} signaling in PC spines and the sensitivity of the peak Ca^{2+} transient to optogenetic-induced MLI excitation. Data from individual spine measurements, in gray, were fit with a linear function ($p = 0.0004$; one-sample t test); binned averages of group data are in black.

All data are mean ± SEM.

paired t test; Figure 2E), consistent with a supralinear increase in Ca^{2+} elevation (Wang et al., 2000). Optogenetic activation of bReaChES-expressing MLIs during the CF stimulus reduced the peak amplitude of the Ca^{2+} response to a level below that produced by CF stimulation alone (Figures 2F and 2G). Interestingly, spines with the largest PF-induced enhancement of CF-evoked intra-dendritic Ca^{2+} elevation were most sensitive to suppression by MLIs (Figure 2H). This is perhaps related to the high precision with which GABA synapses locally control spine Ca^{2+} entry (Chiu et al., 2013). Thus, CF-induced Ca^{2+} signaling in PCs is subject to suppression by MLI-mediated inhibition, even under conditions that increase CF excitability following the conjunctive activity of PFs.

MLI-Mediated Inhibition Influences the Induction of CF-Evoked Synaptic Plasticity

Ca^{2+} signals in PC spines provide a biochemical substrate for inducing diverse forms of synaptic plasticity, including CF-dependent LTD at co-active PF inputs (Finch et al., 2012; Konnerth et al., 1992; Tanaka et al., 2007). Therefore, we explored how the graded suppression of dendritic Ca^{2+} spiking by MLIs influences the induction of activity-dependent plasticity at PF synapses. In the absence of synaptic blockers, test responses to PF stimulation evoked depolarizing postsynaptic potentials (PSPs) in PCs. PSPs reflect the composite influence of both direct PF synaptic excitation and delayed MLI feedforward inhibition (Mittmann et al., 2005). Using a timing rule optimal for inducing PF LTD in the vestibulo-cerebellum (Suvrathan et al., 2016), we observed a long-term (>30 min) decrease in the amplitude of PF-evoked PSPs in floccular PCs following the repeated pairing of PF tetanus in conjunction with CF stimulation (Figures 3A and 3B). Conjunctive pairing also resulted in a lasting decrease in PSP duration (decay, 44.4% ± 11.7% of control; $n = 6$; $p = 0.03$; Wilcoxon matched-pairs test; Figure 3L). Thus, associative CF activity weakens the ability of PFs to excite PCs.

We next used optogenetics to activate ChR2-expressing MLIs ($\lambda = 461$ nm; 20 ms), coincident with CF-evoked excitation of PCs. MLI activity had a significant influence on the induction of

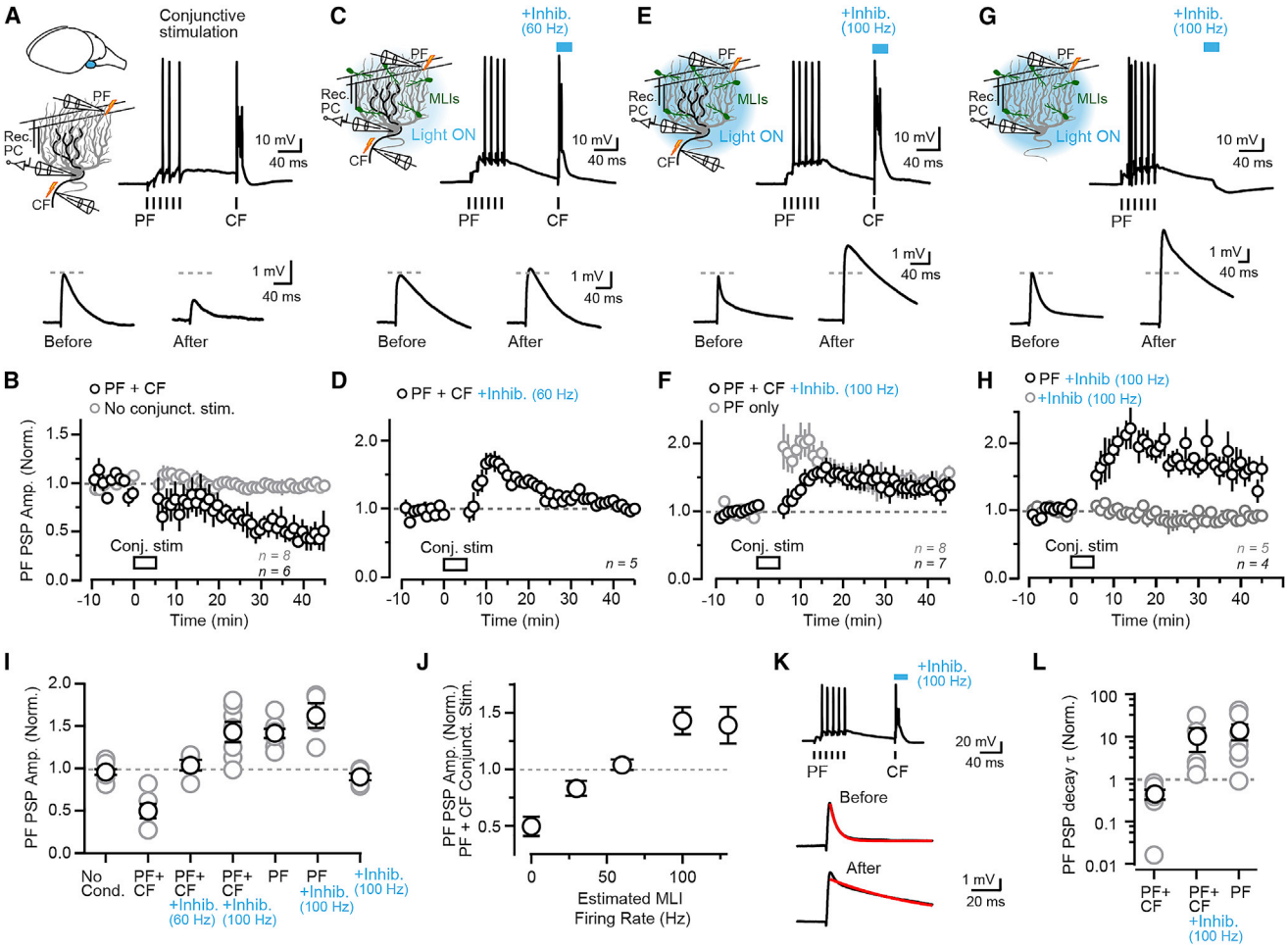

Figure 3. Control of Synaptic Plasticity by MLIs

(A) Pairing protocol used to generate associative plasticity in floccular slices (100 Hz PF tetanus; 60 ms; followed by CF stimulation; 120 ms interval after the 3rd PF stimulus); pairing was repeated 300 times (1 Hz). Below are averaged test PSPs evoked by PF stimulation from the same cell before and after (30–40 min) the pairing protocol.

(B) Plot of the change in test PSP amplitudes across cells normalized to the baseline response for each PC. Paired stimulation led to a lasting decrease in PSP amplitudes (black). Without the conjunctive pairing protocol, PF-evoked PSP amplitudes were stable over time (gray).

(C) Conjunctive CF stimulation occurring coincident with a moderate level of ChR2-induced MLI activation ($\lambda = 461$; 20 ms). Below are averaged test PSPs evoked by PF stimulation from the same cell before and after (30–40 min) the pairing protocol.

(D) After a transient increase in PSP amplitude, test responses to PF stimulation returned to baseline levels following the pairing protocol.

(E) CFs were stimulated coincident with intensive activation of MLIs during the pairing procedure. Below are averaged test PSPs evoked by PF stimulation from the same cell before and after (30–40 min) the pairing protocol.

(F) CF stimulation during the intensive activation of MLIs led to a lasting increase in PF-evoked PSP amplitude (black). A stimulus protocol without CF activation (100 Hz PF tetanus; repeated 300 times; 1 Hz) induced a comparable potentiation of the test PF response (gray).

(G) During the stimulus protocol, MLIs were activated following the PF tetanus (repeated 300 times; 1 Hz).

(H) Delayed MLI activation did not affect the ability of the PF tetanus to induce PSP potentiation (black). Repeated optogenetic activation of MLIs alone did not change PSP amplitude (gray).

(I) Comparison of results across stimulus conditions (individual cells in gray; group average in black; estimated MLI firing rates for optogenetic stimuli are indicated in blue; see Table S2 for statistics).

(J) The influence of increasing levels of MLI activity on the outcome of long-term plasticity stemming from conjunctive PF + CF stimulation during the pairing protocol.

(K) PF-evoked PSPs before and after plasticity induction. MLIs were photostimulated during the CF conjunctive stimulus. Responses were fit with a mono-exponential function (red traces).

(L) Changes in PSP decay time depend on the plasticity-inducing stimulus.

All data are mean ± SEM. See also Figure S4.

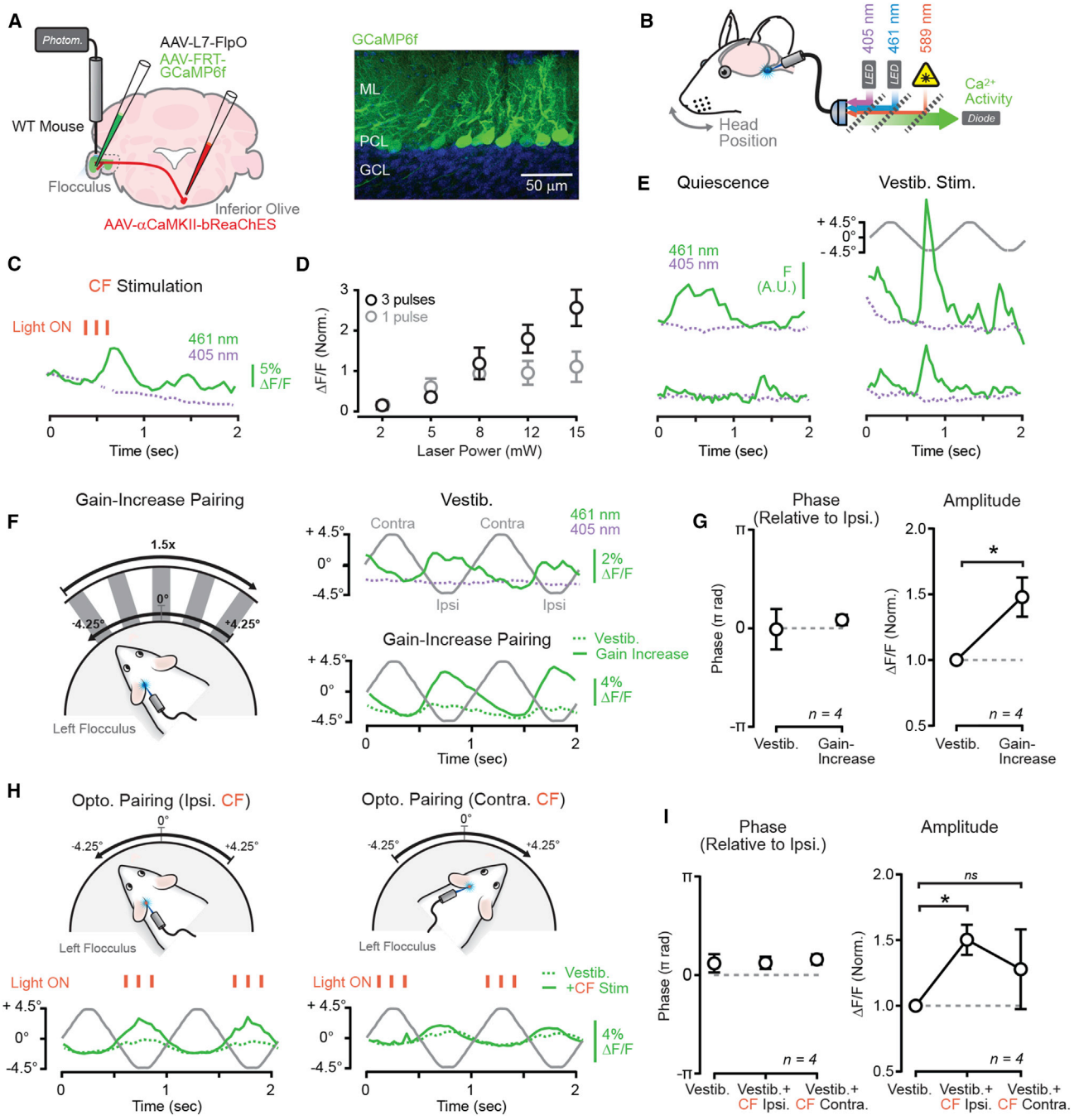

Figure 4. Optogenetic Activation of CFs during Behavior

(A) AAV containing bReaChES was injected in the IO of wild-type (WT) mice to transduce CFs. Floccular PCs were transduced with GCaMP6f using a PC-specific AAV strategy. The confocal image shows the specificity of the viral approach to target PCs.

(B) An implanted optical fiber was used to deliver and collect light for photoactivating CFs and measuring PC Ca^{2+} activity.

(C) Average PC Ca^{2+} response evoked by optogenetic activation of CFs with amber light (3 pulses; $\lambda = 589$; 15 ms; 8 Hz; 8 mW). Laser pulse timing is indicated by the orange tic marks; the concurrent isosbestic measurement is also shown (purple dotted trace).

(D) Relationship between the number and intensity of optogenetic CF stimuli and the evoked Ca^{2+} response in PCs. Data are normalized to the response measured from a single laser pulse at 8 mW.

(E) On the left, Ca^{2+} activity in PCs in quiescent mice; traces are from two different time points. On the right, PC Ca^{2+} activity during different trials of vestibular stimulation to evoke the VOR is shown.

(F) Mice were intermittently subjected to vestibular stimuli with opposite-direction visual motion, a pairing procedure that, if repeated, results in gain-increase adaptation. On the top right, average Ca^{2+} responses in PCs to vestibular stimulation alone (elicited in darkness); concurrent isosbestic measurements (purple

(legend continued on next page)

long-term associative plasticity. When CFs were stimulated coincident with moderate levels of MLI activity, there was no longer a lasting change in the amplitude of PF-evoked PSPs (Figures 3C, 3D, and 3I). This indicates that expression of long-term plasticity was occluded by MLI-mediated inhibition. In contrast, conjunctive CF stimulation during intensive MLI activation yielded the opposite form of synaptic plasticity: long-term potentiation of PF-evoked PSP amplitude (Figures 3E, 3F, and 3I) and duration (decay, 1,021.0% ± 580.2% of control; n = 5; p = 0.03; Wilcoxon matched-pairs test; Figures 3K and 3L). This effect was reminiscent of non-associative LTP elicited at PF-PC synapses when PFs are repeatedly activated independent of CFs (Figures 3F, 3I, and 3L; Lev-Ram et al., 2002), indicating that high levels of MLI activity fully negate the associative role of CFs. Specifically, CF co-activation no longer induced plasticity that weakened PF excitation of PCs. Instead, MLI activity allowed for PF-evoked strengthening of PF responses. The efficacy of the PF tetanus in inducing long-term potentiation was unaffected by delayed optogenetic activation of MLIs that was timed to replace the omitted CF conjunctive stimulus (Figures 3G–3I). This suggests a lack of direct interaction between inhibition from MLIs and the response to PF activity leading to plasticity. Because repetitive optogenetic activation of MLIs alone failed to alter PSP amplitude (Figures 3H and 3I), the MLI-induced reversal in the polarity of plasticity was not due to an indirect effect of MLIs on membrane excitability.

Plasticity rules were also evaluated with $GABA_A$-receptor-mediated inhibition blocked (SR 95531; 20 μM). In this condition, conjunctive activation of PFs and CFs generated LTD (PSP amplitude, 84.8% ± 9.3% of control; n = 11; p = 0.04; paired t test), though the plastic change in PSP amplitude in this condition was less than with inhibition intact (p = 0.02; unpaired t test). This effect likely is attributable to the influence of feedforward MLI inhibition, and its plastic adjustment, on setting PSP amplitude (Mittmann and Häusser, 2007; Mittmann et al., 2005) rather than an underlying influence of tonic MLI activity on CF-evoked PC Ca^{2+} signaling. In contrast, LTP induction by the PF tetanus alone (PSP amplitude, 161.6% ± 18.5% of control; n = 7; p = 0.001; paired t test) elicited a similar change in PF strength relative to measurements obtained with MLI activity unblocked (Figures 3F and 3I; p = 0.29; unpaired t test). Interestingly, in the absence of inhibition, changes in PSP duration following plasticity induction were greatly reduced or absent (Figures S4A and S4B). Together, these results point to the potential role of MLIs in plasticity-induced changes in PSP amplitude and kinetics, a plasticity that was also susceptible to modulation through inhibitory regulation of CF-evoked PC Ca^{2+} signaling.

In summary, plasticity changed along a continuum that depended on the level of MLI inhibition during CF excitation: responses were weakened when CFs were stimulated in the absence of optogenetic MLI-mediated inhibition, whereas responses were strengthened when CFs were excited coincident with intensive MLI activity (Figure 3J). Thus, the graded influence of MLI activity on dendritic spiking and Ca^{2+} elevation in PCs can produce a wide variety of plasticity outcomes, potentially enhancing the computational role of CFs in instructive signaling.

Optogenetic Activation of CFs during the VOR

LTD and LTP at PF synapses are thought to serve as the cellular basis for encoding learning that strengthens or weakens adaptive movements (Boyden et al., 2004; Boyden and Raymond, 2003). By strongly regulating dendritic Ca^{2+} signaling and, hence, plasticity at PC synaptic inputs, MLIs are poised to influence how motor learning is acquired. We evaluated this possibility *in vivo* by using adaptation of the VOR as a behavioral readout of cerebellar-dependent motor learning. When confronted with the lack of image stability, the VOR undergoes learned changes in amplitude (gain) to restore distortion-free performance, due to activity in the cerebellar flocculus (Ito, 1982). In particular, image slippage on the retina indicates motor performance error and triggers instructive signals through the activity of CFs. To directly establish the causal effect of CF activity on VOR gain adaptation, we used optogenetic stimulation of CFs in place of visual motion to artificially drive motor learning (Kimpo et al., 2014). For this approach, AAV containing the red-shifted opsin bReaChES under control of the αCaMKII promoter was injected into the IO (Figures S5A and S5B). Prominent transduction of IO excitatory projection neurons was evidenced by high-efficiency transgene expression in floccular CFs and a scarcity of labeled mossy fibers (Figures S5C and S5D).

We next determined if optogenetic CF excitation was effective at manipulating PC Ca^{2+} activity *in vivo*. Thus, to record CF-evoked activity in PCs, we expressed the Ca^{2+} sensor GCaMP6f (Chen et al., 2013) specifically in these cells using a viral strategy. AAV containing the recombinase FlpO under control of a truncated version of the *L7/Pcp2* promoter (Nitta et al., 2017) was co-injected with a second, FlpO-dependent GCaMP6f-containing AAV (Figure 4A). PC population responses were measured using fiber photometry in the flocculi of head-fixed, awake mice held in darkness (Figure 4B). Optogenetic activation of bReaChES-expressing CFs elicited time-locked increases in PC Ca^{2+} activity (Figure 4C). The peak amplitude of the evoked Ca^{2+} response increased with the number and intensity of the optogenetic stimuli (Figure 4D).

dotted trace) show the absence of motion artifacts. On the bottom right, responses with and without visual pairing during the vestibular stimulus are superimposed (solid and dotted green traces, respectively). Vestibular stimuli are indicated in gray.

(G) Comparison of the phase (relative to the end of ipsiversive head movements) and amplitude of peak PC Ca^{2+} activity during the vestibular stimulus and that induced with visual-vestibular pairing that eventually leads to gain-increase adaptation. *p < 0.05; paired t test.

(H) The same mice were also intermittently subjected to pairing of vestibular stimuli with optogenetic activation of CFs in association with completion of either ipsiversive or contraversive head turns (in darkness). Average PC Ca^{2+} activity measurements during CF pairing (green trace) are shown superimposed with responses evoked by the vestibular stimulus alone (green dotted trace).

(I) Summary data showing the effect of phase-specific, optogenetic CF activation on modulation of PC Ca^{2+} activity evoked by vestibular stimulation. *p < 0.05; one-way repeated-measures ANOVA with Bonferroni post-test.

All data are mean ± SEM. See also Figures S5 and S6.

During quiescence, robust Ca^{2+} activity was apparent in PCs of awake mice (Figure 4E), perhaps owing to the regular firing of CFs. However, on average, PC Ca^{2+} activity was coherently modulated when mice were subjected to passive sinusoidal vestibular stimuli (1 Hz; ±8.5°; 22°/s peak velocity) to trigger the VOR (Figures 4E and 4F). Ca^{2+} responsiveness was positively modulated for ipsiversive movements (i.e., for PCs in the left flocculus, activation was the greatest for leftward head turns), starting during the peak phase of motion and ending with the completion of the movement (Figures 4F and 4G). Concurrent isosbestic measurements (Kim et al., 2016) showed that Ca^{2+} signal modulation was not the result of motion artifacts (Figure 4F). To determine how PC Ca^{2+} activity was altered by retinal slip, we interleaved infrequent trials where vestibular stimuli were paired with opposite-direction visual motion (1.5× visual-vestibular stimulus; Figure 4F). PC Ca^{2+} activity was greatly enhanced by this stimulus without change to the timing of the peak evoked response compared to that induced by vestibular stimulation alone (Figure 4G).

For the VOR, opposite-direction visual-vestibular pairing is an adaptation-inducing stimulus that is thought to depend on modulation of CF activity during ipsiversive head turns (Ke et al., 2009). The effectiveness of CFs at modulating PC Ca^{2+} activity was tested by stimulating bReaChES-expressing CFs during the VOR (Figure 4H). Optogenetic activation of CFs (λ = 589; 3 pulses; 15 ms; 8 Hz; 8 mW; in darkness) near the end of ipsiversive vestibular stimulation led to an increase in the PC Ca^{2+} response (Figures 4H and 4I). Thus, optogenetic CF activation at the peak position of the movement, when the behavioral-induced Ca^{2+} response was complete, produced an additive Ca^{2+} signal. However, the PC Ca^{2+} response evoked by vestibular stimulation was not significantly altered by CF activation for contraversive head movement (Figures 4H and 4I). Similar results were obtained when CFs were activated during the peak phase of head velocity during turns; ipsiversive stimuli produced enhancement of vestibular Ca^{2+} signals, comparable to that produced by opposite-direction visual motion, although contraversive stimuli had no effect on these responses (Figures S6A and S6B). Interestingly, although optogenetic CF stimuli were effective at producing Ca^{2+} signals during ipsiversive head movements, the same stimuli timed to completion of contraversive motion failed to evoke a concomitant Ca^{2+} response during this period (i.e., activation of CFs in the left flocculus was impotent for rightward head turns; ΔF/F 103.9% ± 20.1% of control trials; p = 0.86; paired t test; Figure 4H). This suggests that the ability of CFs to modulate PC Ca^{2+} signaling was prevented during this context of vestibular stimulation. In summary, optogenetic stimulation of CFs was effective at inducing Ca^{2+} activity in PCs and could be used to mimic learning-induced signals evoked by motor performance errors.

Dual-Color Optogenetic Actuation of CFs and MLIs

To directly establish the causal effect of MLI activity on CF Ca^{2+} signals that instruct VOR gain adaptation, we used a dual-color optogenetic strategy to independently excite CFs with and without coincident MLI activation. To accomplish this, AAV containing bReaChES was injected in the IO of nNOS-ChR2 mice (Figure 5A). In acute cerebellar slices prepared from IO-injected nNOS mice, wide-field illumination of bReaChES with amber light (λ = 596 nm; 5 ms) induced complex spikes in PCs (3.5 ± 0.3 spikelets per burst) that were indistinguishable from those elicited by electrical stimulation of CFs (3.8 ± 0.5 spikelets per burst; n = 5; p = 0.39; paired t test; Figures 5B and 5C). The probability of eliciting a complex spike saturated with increasing light power; stereotyped responses were produced independent of stimulus intensity or duration (Figures 5D, S7A, and S7B). Complex spikes could be evoked with high reliability using bReaChES excitation, even during frequent, repetitive CF stimulation (3 pulses; 8 Hz; repeated at 1 Hz; Figure S7C). Although blue light (λ = 461 nm; 20 ms) was relatively inefficient at exciting CFs at low powers ($\leq$2 mW/mm^2), complex spikes could be evoked with high power (>5 mW/mm^2; Figures 5E, 5F, and S7D), as expected from the broad action spectrum of bReaChES (Rajasethupathy et al., 2015). MLIs expressing blue-light-sensitive ChR2 were not directly activated by amber light at high powers (9.4 mW/mm^2; 200 ms; Figure 5G). Neither were granule cells (Figures S5E and S5F), supporting the conclusion that mossy fibers generally did not express bReaChES. However, in the absence of synaptic blockers, amber light could produce weak excitation of MLIs, detected as an increase in spike probability, time-locked to the stimulus, during cell-attached recordings (Figure 5H). This response is attributable to spillover-mediated excitatory transmission from CFs onto MLIs (Coddington et al., 2013; Mathews et al., 2012; Szapiro and Barbour, 2007).

When bReaChES-induced CF excitation of PCs (λ = 596; 5 ms) coincided with ChR2-mediated inhibition by MLIs (λ = 461 nm; 20 ms), we observed no effect on spikelet content during the somatic complex spike across a range of MLI activity levels (Figures 5E and S7E). However, Ca^{2+} spiking in the dendrite was suppressed by MLI-mediated inhibition (Figures 5I and 5J). This effect was abolished in the presence of $GABA_A$ receptor block (2.75 ± 0.25 and 2.75 ± 0.25 Ca^{2+} spikes in dendritic burst, CF alone, and CF + MLI inhibition, respectively; n = 4; p = 1.0; paired t test; Figure 5K). These results show the effectiveness of our dual-color optogenetic approach in actuating CFs independent of MLIs. Moreover, through the coincident pairing of CF excitation with that of MLIs, optogenetics could selectively control Ca^{2+} spiking in PC dendrites independent of complex spiking in the soma.

Control of CF-Evoked Learning by MLI-Mediated Inhibition

We used our dual-color optogenetic approach to examine how MLI activity influences CF-evoked learning in the performance of the VOR. We first tested the ability of optogenetic CF activity to induce long-term VOR adaptation. In IO-injected nNOS-ChR2 mice (Figure 6A), bilateral floccular activation of bReaChES-expressing CFs with amber light (λ = 589; 3 pulses; 15 ms; 8 Hz; 8 mW) occurred in association with the completion of the ipsiversive phase of sinusoidal vestibular motion (1 Hz; ±8.5°; 22°/s peak velocity; 30 min; i.e., CFs in the left and right flocculi were alternately photostimulated near the end of leftward and rightward head movements, respectively; Figure 6B). This timing allowed optogenetic-induced CF Ca^{2+} signals in PCs to follow PF firing during the vestibular stimulus, as well as avoid direct interaction with the

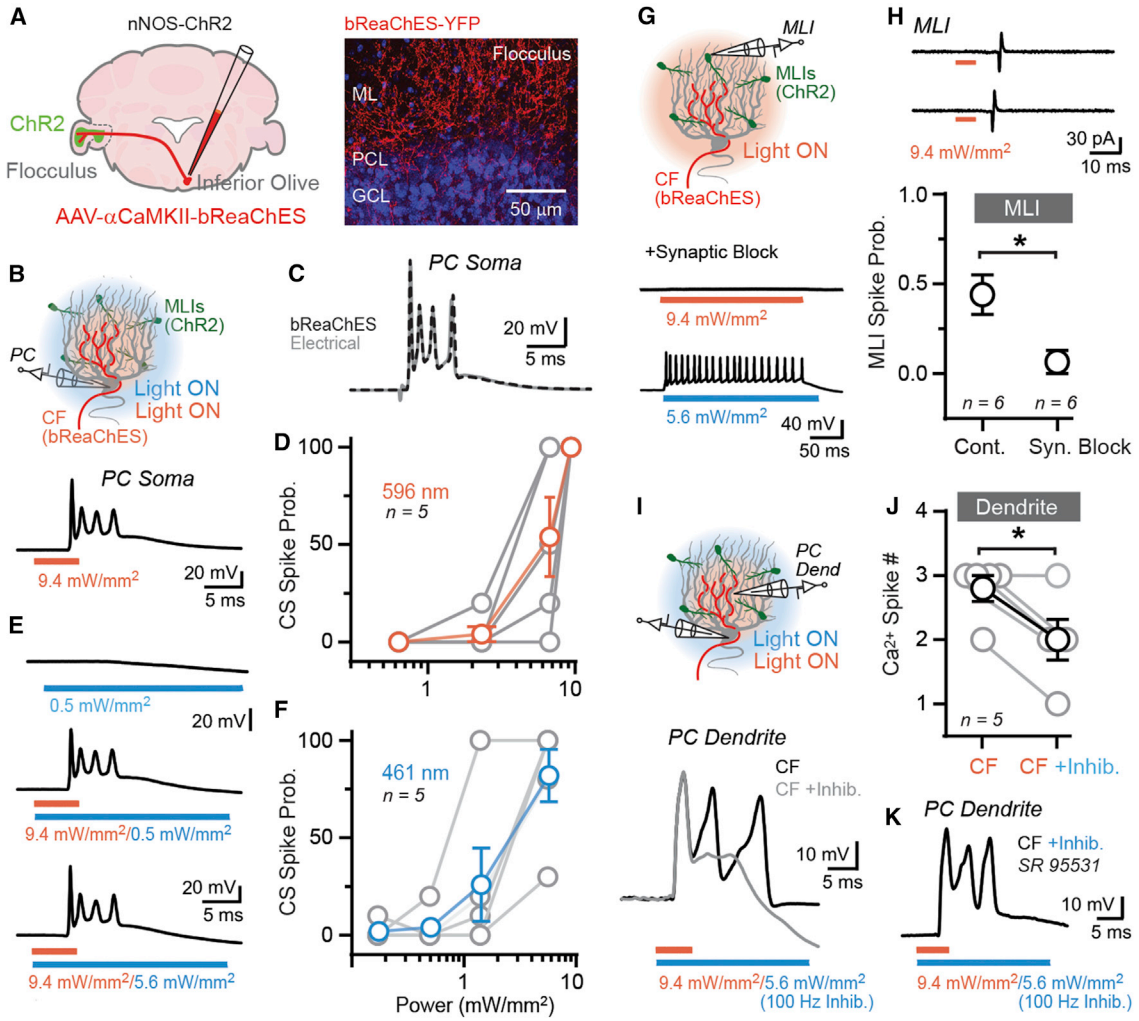

Figure 5. Dual-Color Optogenetic Control of CFs and MLIs

(A) In nNOS-ChR2 mice, AAV containing bReaChES was injected in the IO, resulting in expression in floccular CFs.

(B) Somatic complex spike evoked in a PC following optogenetic activation of CFs with amber light.

(C) Superimposed complex spikes in the same PC evoked by either optogenetic or electrical stimulation of the CF.

(D) Probability of evoking a complex spike in PCs increased with the power of amber light.

(E) In a slice recording from a nNOS-ChR2 mouse, the responsiveness of a PC to optogenetic activation of bReaChES-expressing CFs to blue light alone (top) or in combination with amber light at low (middle) or high (bottom) blue-light powers.

(F) With high powers, blue-light excitation of bReaChES-expressing CFs evoked complex spikes in PCs.

(G) Direct optogenetic excitation of a ChR2-expressing MLI by blue light; the cell was insensitive to amber light.

(H) In the absence of synaptic blockers, CF excitation with amber light drove infrequent spiking in MLIs. *p = 0.02; unpaired t test.

(I) In a PC dendritic recording, Ca^{2+} spiking induced by optogenetic CF activation in control (black) or during the coincident photo-activation of ChR2-expressing MLIs (gray).

(J) The effect of MLI activation (blue light) on optogenetic CF-evoked dendritic spiking (amber light). *p = 0.02; paired t test. Within-cell comparison is in gray; group average is in black.

(K) Suppression of bReaChES-induced Ca^{2+} spiking by ChR2 activation of MLIs was abolished by the $GABA_A$ receptor blocker SR 95531 (20 μM).

All data are mean ± SEM. See also Figures S5 and S7.

behavior-induced Ca^{2+} response that began at the peak phase of head velocity. Also, to eliminate instructional signals associated with retinal slip cues, optogenetic pairing was performed in the dark. However, in darkness, vestibular stimulation alone (in absence of any visual stimulus and/or optogenetic activity) results in a decrease in VOR gain (Stahl, 2004). This habituation could be measured and fully accounted for using control sessions of vestibular-only stimulation in the same mice (Nguyen-Vu et al., 2013).

Pairing CF activity with the completion of ipsiversive head movement resulted in an increase in VOR gain relative to the vestibular-only control condition (Figures 6D, 6E, and 6H). The learned response elicited by optogenetic CF activation

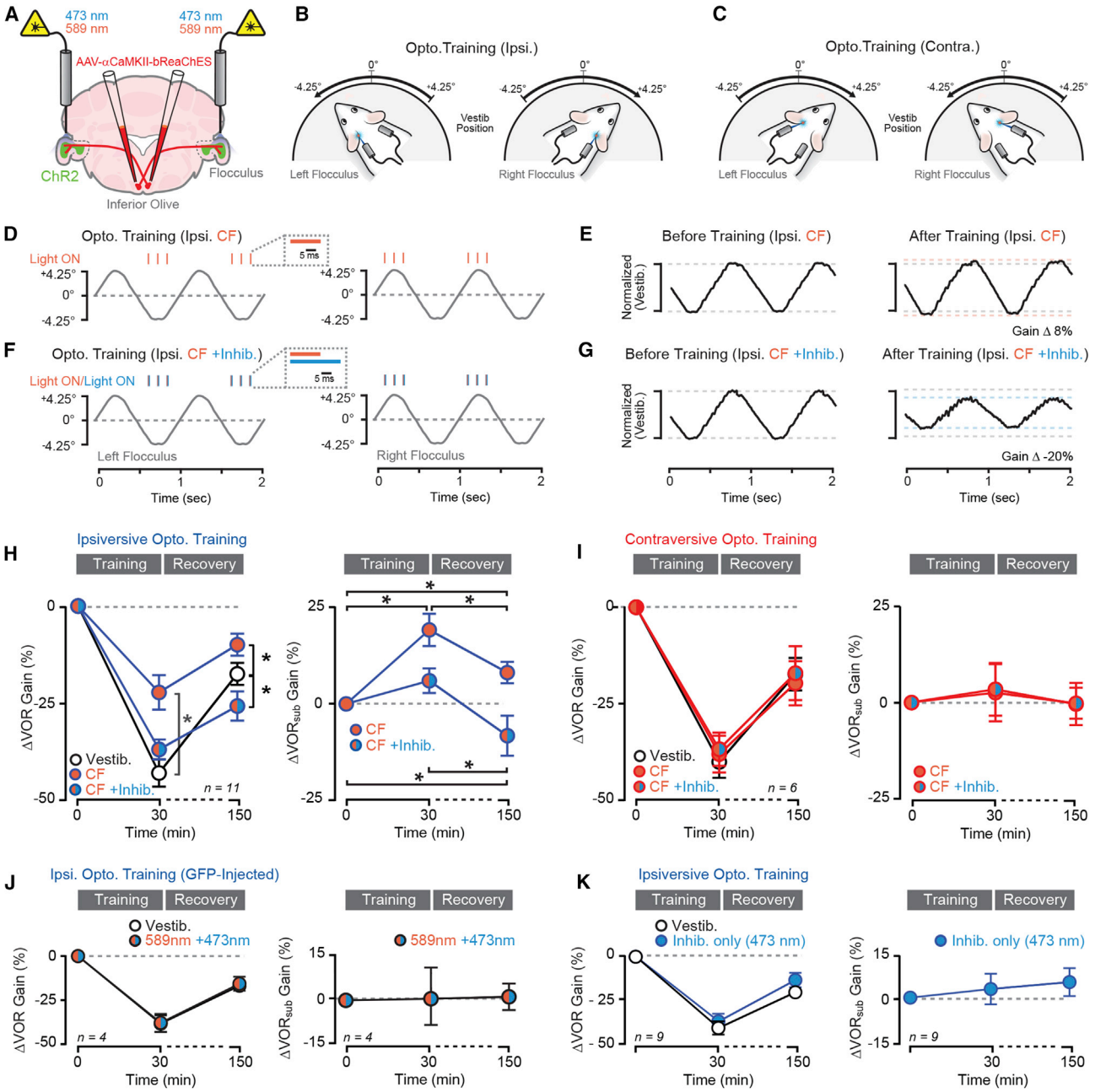

Figure 6. Alteration of CF-Evoked Motor Learning by MLI Activation

(A) Optical fibers targeting both flocculi were implanted into nNOS-ChR2 mice. CFs expressed bReaChES by AAV-mediated transduction of the IO.

(B) Over the course of training, floccular CFs were activated with amber light in association with completion of ipsiversive head turns during sinusoidal vestibular stimulation. In alternative training sessions, CFs were activated coincident with MLIs by concomitant pulses of blue light.

(C) Training paradigm with associative pairing of optogenetic activity with contraversive head movements.

(D) Timing of laser pulses for CF activation relative to the vestibular stimulus (gray) for both flocculi during ipsiversive optogenetic training.

(E) Average VOR-evoked eye movements measured before and after training. The traces were normalized to that of time-matched, control responses recorded during sessions of vestibular stimulation alone.

(F) Dual-color optogenetic stimulation of CFs and MLIs during training.

(G) Average VOR-evoked eye movements from the same mouse shown above but with CF activation coincident with that of MLIs during training.

(H) Summary plots showing the effect of MLI-mediated inhibition on artificial motor learning produced by CF stimulation in association ipsiversive movements. VOR performance was measured in the dark to head rotation at the beginning and ending of training as well as after holding mice in the dark for 120 min during the post-training recovery period. A training session of vestibular stimulation alone controlled for darkness-induced habituation. In the first plot, motor learning is quantified as the change in VOR amplitude after training relative to baseline performance (ΔVOR gain). In the second plot, the subtracted difference of sessions

(legend continued on next page)

resembled gain-increase adaptation induced by motor performance errors during opposite-direction visual-vestibular training known to recruit CF activity during ipsiversive head movements (Raymond and Lisberger, 1998). Similar results were obtained using optogenetic CF activation timed with the peak phase of ipsiversive head velocity (Figures S8A and S8C), a stimulus that more closely approximated the endogenous modulation of CFs by opposite-direction visual motion (Ke et al., 2009). In contrast, optogenetic CF pairing with the completion of contraversive head movements failed to produce a change in the VOR beyond darkness-induced habituation (Figures 6C and 6I). Thus, the ability of CFs to instruct motor learning in the VOR depends on sensorimotor context (Kimpo et al., 2014; Nguyen-Vu et al., 2013).

We also used dual-color optogenetics to elicit CF excitation (λ = 589; 3 pulses; 15 ms; 8 Hz; 8 mW) coincident with activation of MLIs (λ = 473; 25 ms; 8 Hz; 2 mW; Figure 6F) in separate training sessions in the same mice. Using this regimen, the associative activity of CFs with ipsiversive vestibular stimulation failed to produce a relative increase in the VOR. Instead, for stimuli timed to the end of movement, there was lasting reduction in VOR gain compared to the change recorded in the vestibular-only control condition (Figures 6G and 6H). Therefore, CF activation coincident with MLI-mediated inhibition could induce a learned VOR response in the direction opposite that produced by CF activation alone. Although, for dual-color optogenetic stimuli occurring during the peak phase of ipsiversive head velocity (Figure S8B), a lasting reduction relative to the vestibular-only condition was not observed. However, CF-induced changes were apparent when these inputs were stimulated alone in this condition (Figure S8C), indicating that MLIs could gate CF-evoked adaptation during their coincident stimulation. Thus, the precise timing of CF and MLI co-activity during head turns could determine the overall influence of inhibition on learning outcomes.

VOR performance remained unaltered, relative to measurements in control sessions, when MLI stimulation occurred coincident with optogenetic CF activation for contraversive head movements (Figure 6I). This indicates that MLI activation does not alter the context dependence of CF-mediated learning. Likewise, pairing ipsiversive head movements with dual-color illumination in mice injected with GFP in place of the optogenetic actuators failed to induce an appreciable change in VOR performance, apart from darkness-induced habituation (Figure 6J). This demonstrates that the outcome of learning induced by optogenetic activation of CFs was unrelated to the light stimulus itself. During pairing, optogenetic-induced neural activity did not contribute directly to eye movements evoked by the VOR with short latency (Figures S9A and S9B). This indicates that adaptation induced by optogenetics was not due to perturbation of the behavioral response to vestibular stimulation.

To control for the possibility that MLI activation produced learning through modulation of PC simple spiking (Lee et al., 2015), we also examined for changes in the VOR induced by pairing blue light optogenetic activation (λ = 473; 25 ms; 8 Hz; 2 mW) with the completion of ipsiversive head movements. However, there was no lasting effect of this training on VOR performance compared to measurements in control sessions (Figure 6K). Our *ex vivo* experiments showed that blue light used to excite MLIs could potentially activate bReaChES-expressing CFs when using high-intensity light powers (see Figure 5F). Therefore, we also performed optogenetic pairing experiments in *c-kit::Cre* mice injected with AAV containing Cre-dependent ChR2 as an additional control. Again, we found that MLI activation in association with the end of ipsiversive head movements (λ = 473; 1 pulse; 240 ms; 0.5–10 mW; 30 min) failed to adapt the VOR beyond the darkness-induced change measured in control sessions (ΔVOR −40.5% and −38.3% of baseline; control and ipsiversive stimulation, respectively; n = 5; p = 0.50; paired t test). The effectiveness of PC simple spike modulation in instructing learning may require longer duration training regimes than those used in our experiments (e.g., >30–60 min; see Medina, 2011) or a greater level of optogenetic activation to fully silence PCs during vestibular stimulation. Together, these results suggest that MLIs potently modulate the PC response to CF excitation and, through their effect on the selection of plasticity, help determine learning valence.

MLI Control of VOR Learning Induced by Retinal Slip

Learning elicited by optogenetic activation of CFs with ipsiversive head movement is likely a mechanistic proxy for gain-increase adaptation produced by retinal slip occurring during visual motion in the direction opposite to vestibular stimulation (Boyden and Raymond, 2003; Kimpo et al., 2014). Therefore, if optogenetic-induced MLI activity affects the outcome of CF-mediated learning, then a visual-vestibular pairing that produces gain-increase adaptation should be sensitive to the addition of MLI-mediated inhibition. To examine this question, we paired vestibular stimulation (1 Hz; ±5.0°; 20°/s peak velocity; 60 min) with opposite-direction visual motion (1.5× visual-vestibular stimulation) and used blue light to activate ChR2-expressing MLIs in AAV-injected *c-kit::Cre* mice during training (Figure 7A). Bilateral activation of floccular MLIs (λ = 473; single 240 ms pulse; 0.5–10 mW) occurred in an alternating pattern for each side of the head, timed with the peak phase of head velocity when PC Ca^{2+} activity was positively modulated by visual-vestibular stimulation.

MLI activation significantly altered how learning was acquired. Instead of causing an increase in VOR gain, as observed in control sessions (Figures 7B, 7C, and 7H), mice adapted their

with and without optogenetic stimulation shows the isolated effect of CF activation on VOR performance. *p < 0.05; two-way repeated-measures ANOVA with Bonferroni post-test.

(I) Results obtained for training with CF activation in association with the end of contraversive head turns.

(J) Concomitant pulses of amber and blue light in association with the completion of ipsiversive movements had no effect on VOR performance, relative to control measurements, in *c-kit::Cre* mice injected with GFP-containing AAVs in place of optogenetic actuators.

(K) Similarly, pairing optogenetic MLI activation with blue-light pulses with the end of ipsiversive head movements did not change VOR performance beyond darkness-induced habituation.

All data are mean ± SEM. See also Figures S8 and S9.

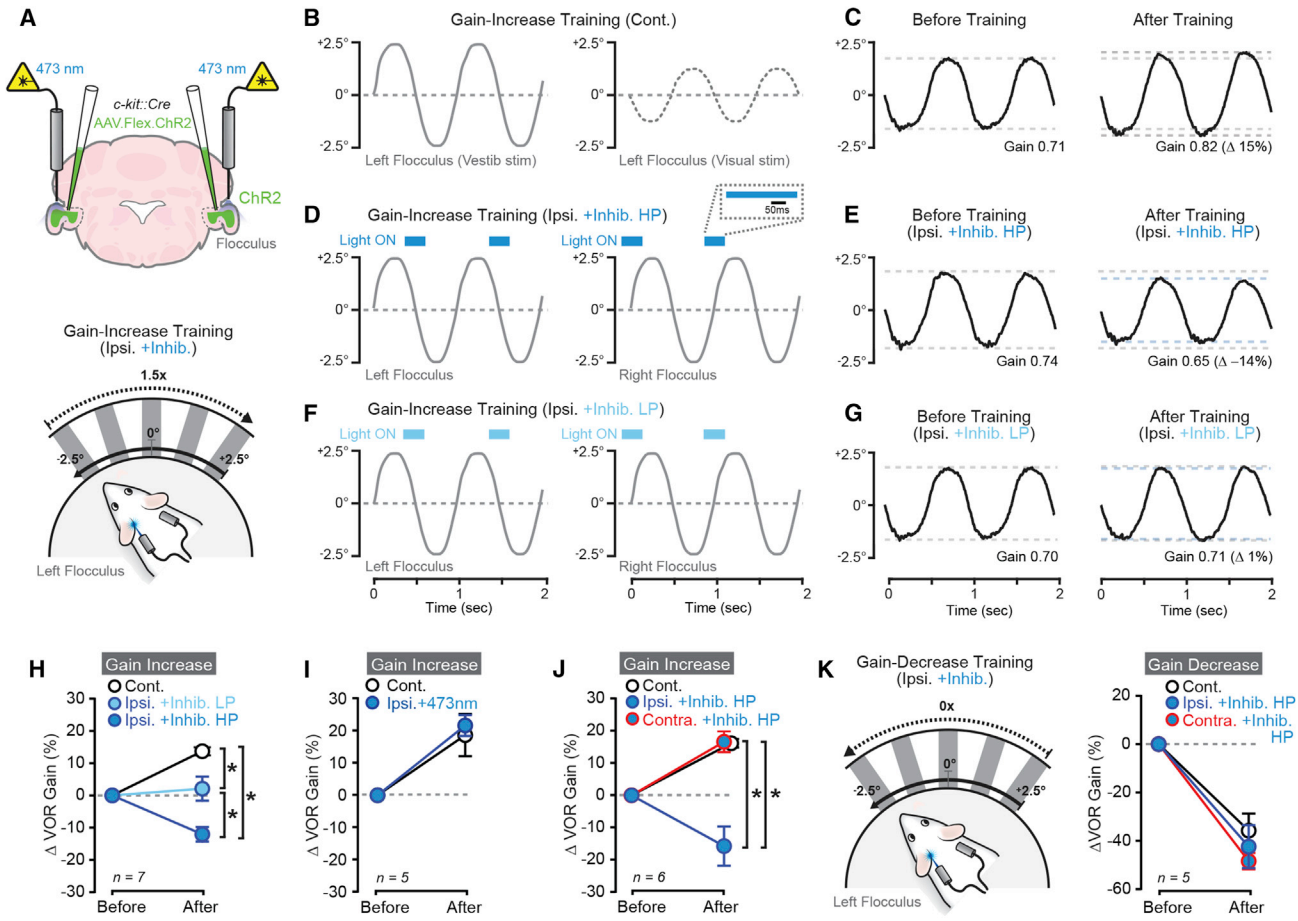

Figure 7. Optogenetic Activation of MLIs Affects the Outcome of VOR Learning Induced by Retinal Slip

(A) MLIs in *c-kit::Cre* mice were transduced with ChR2; optical fibers targeted both flocculi. Shown below is opposite-direction visual-vestibular pairing with optogenetic activation of MLIs.

(B) Control sessions of training consisted of pairing head rotation (solid gray) and opposite-direction visual motion (dotted gray) without optogenetic activity.

(C) Average VOR-evoked eye movements before and after training.

(D) During opposite-direction visual-vestibular pairing that normally leads to gain-increase adaptation, laser pulses used to activate MLIs (in blue) occurred with the peak phase of ipsiversive head velocity during sinusoidal stimulation.

(E) VOR-evoked eye movements from the same mouse as above but with optogenetic activation of MLIs during the pairing procedure.

(F) Mice were retrained using a lower power laser stimulus for activating MLIs.

(G) Comparison of average VOR eye movements before and after visual-vestibular pairing with low-power laser stimuli.

(H) The effect of optogenetic-induced MLI activity on opposite-direction visual-vestibular pairing on VOR learning. Two different stimulus intensities were used during pairing (HP and LP; high and low power, respectively; determined for each mouse; STAR Methods). *p < 0.05; two-way repeated-measures ANOVA with Bonferroni post-test.

(I) Photostimulation of floccular MLIs in *c-kit::Cre* mice injected with AAV containing GFP occurred following ipsiversive head movements during opposite-direction visual-vestibular pairing.

(J) Summary results from a second cohort of animals showing the phase-specific influence of MLI activity on learning during gain-increase training. *p < 0.05; two-way repeated-measures ANOVA with Bonferroni post-test.

(K) Optogenetic activation of MLIs had no effect on gain-decrease learning produced during vestibular pairing with same-direction visual motion.

All data are mean ± SEM. See also Figure S9.

VOR with an opposite valence. The gain of their VOR decreased with MLI activation during pairing (Figures 7D, 7E, and 7H). Retraining the mice in a separate session with a lower-power optogenetic stimulus (0.3–5 mW) produced an intermediate effect on the VOR: that is, the absence of adaptation (Figures 7F–7H). VOR-evoked eye movements during visual-vestibular pairing that included MLI activation were no different than trials without the optogenetic stimulus, indicating that alteration of learning outcome was not the result of an acute behavioral perturbation (Figure S9C). Furthermore, control experiments in *c-kit::Cre* mice injected with AAV containing Cre-dependent GFP showed normal gain-increase adaptation, indicating that optogenetic-induced alteration of learning was not an artifact of the light stimulus (Figure 7I). The influence of MLI activity on

VOR adaptation was context dependent. Gain-increase learning was unaffected with optogenetic-induced inhibition occurring during the peak phase of head velocity for contraversive head movements (Figure 7J), a period of the VOR absent for PC Ca^{2+} activity modulation during visual-vestibular pairing. These results are consistent with the gating effect MLI activity has on the valence of artificial VOR learning produced by optogenetic activation of CFs. Thus, under naturalistic learning conditions, MLI stimulation progressively overrides the ability of CFs to instruct an appropriate plasticity to accurately correct VOR performance.

The gain of the VOR is bidirectionally modulated by visual-vestibular training (Ito, 1982). Head rotation repeatedly paired with same-direction visual motion (Boyden and Raymond, 2003; 1 Hz; ±5.0°; 20°/s peak velocity; 0× visual motion; 60 min) produces a learned decrease in VOR performance (Figure 7K). Interestingly, gain-decrease VOR learning was unaffected by phasic activation of MLIs by ChR2 timed with the peak velocity of ipsiversive or contraversive head turns (Figure 7K). This suggests that the instructive signals that underlie this form of learning are resistant to the addition of optogenetic MLI activity. In conclusion, the valence of VOR adaptation produced during instructive signaling by CFs, driven by motor performance errors, is altered in a graded manner by coincident optogenetic-induced MLI activity. This indicates a potential role for MLI-mediated inhibition in gating instructive signaling. Ultimately, this mechanism could ensure the appropriateness or accuracy of learning during different behavioral contexts.

DISCUSSION

Our findings substantially broaden the understanding of rules that govern cerebellar function during the acquisition of motor learning. We find that MLIs can suppress CF-evoked Ca^{2+} spiking in PC dendrites to produce graded Ca^{2+} signals. By regulating dendritic Ca^{2+} signaling, MLIs exert a potent influence on the strength and polarity of activity-induced synaptic plasticity, thereby altering the ability of PFs to excite PCs. The modulatory effect of inhibition by MLIs on synaptic plasticity expands the range over which CF-mediated instructive signaling can guide learning, in part determining the magnitude and valence of adapted motor responses. This permits a wider spectrum of learning outcomes that modify behavior.

MLI-Mediated Inhibition Modulates Dendritic Ca^{2+} Spiking in PCs

We found that $GABA_A$-receptor-mediated inhibition reduces the number and amplitude of dendritic Ca^{2+} spikes in a CF-evoked burst and, thereby, diminishes intracellular Ca^{2+} signals. This process likely involves membrane hyperpolarization produced by $GABA_A$ receptor activation that increases the availability of voltage-gated K^+ channels expressed on PC dendrites, preventing Ca^{2+} spike initiation and propagation (Otsu et al., 2014). Shunting inhibition can also contribute to reduced membrane excitability, and its role in Ca^{2+} spike suppression cannot be ruled out (Callaway et al., 1995). The suppressive action of MLIs on dendritic Ca^{2+} elevation was positively correlated with the level of MLI activity. Thus, the integration of MLI inhibitory input by the PC dendrite during CF excitation permits graded Ca^{2+} responses to extend the range of an instructive stimulus beyond a binary all-or-none event (Eccles et al., 1966).

In PCs, complex spikes are initiated in the axon independent from the influence of Ca^{2+} spike genesis in the proximal dendrite (Davie et al., 2008; Otsu et al., 2014). Therefore, when MLIs were synchronously activated by brief optogenetic stimuli, inhibitory suppression of dendritic Ca^{2+} spiking occurred without affecting the complex spike waveform in the soma. This is similar to results reported for non-selective stimulation of MLIs (Callaway et al., 1995). Because PCs integrate convergent input from many MLIs (Kim et al., 2014), branch-specific regulation of dendritic spiking by localized inhibition may be possible during weak or sparse activation of MLIs. However, *in vivo* measurements in awake mice show that MLIs are densely recruited in a coherent and robust manner during motor behavior (Chen et al., 2017; Gaffield and Christie, 2017; Jelitai et al., 2016). This favors a uniform influence of MLI-mediated inhibition on Ca^{2+} spike suppression across the entire PC dendritic arbor.

In awake rodents, both CFs and MLIs are activated during movement (Chen et al., 2017; Gaffield et al., 2016; Gaffield and Christie, 2017; Jelitai et al., 2016). However, the relative timing of their co-activity is unclear. Thus, we do not know whether MLIs suppress PC dendritic spiking during motor output and, if so, whether behavioral context plays a role in the dynamics of their interaction. Graded control of dendritic Ca^{2+} spiking has been shown *in vivo* (Najafi et al., 2014a, 2014b). This suggests that the integrated dendritic response of PCs to CF activity contains information pertaining to movement-related sensorimotor variables that modulate the magnitude of putative instructive stimuli. Further work will be necessary to examine whether MLI activity is involved in this signaling process.

MLI-Mediated Inhibition Shapes the Induction of Synaptic Plasticity

Opposite-direction synaptic plasticity affects the ability of PFs to modulate PC simple spiking by changing the strength of their excitatory and inhibitory connections. The activity of CFs plays a significant role in determining the type of plasticity produced at these locations. LTD at PF-PC synapses depends on the associative activity of CFs (Ito and Kano, 1982), whereas LTP results when PFs are repetitively activated at high frequency in the absence of CF activity (Lev-Ram et al., 2002). MLI synapses, between both PFs and PCs, have also been implicated as sites of plasticity but with LTD and LTP at these sites having an opposite dependence on CFs (Jörntell and Ekerot, 2002, 2003; Kano et al., 1992; Rancillac and Crépel, 2004). Selective induction of distinct plasticity mechanisms likely results from different patterns of Ca^{2+} signaling in PC dendrites. PF activity alone produces a relatively modest increase in Ca^{2+}, whereas their co-activation with CFs results in an enhanced Ca^{2+} elevation greater than CF excitation alone (Piochon et al., 2016). These Ca^{2+} signaling regimes differentially engage Ca^{2+}-dependent kinases and phosphatases that direct receptor composition and abundance at synapses (Lamont and Weber, 2012).

By suppressing dendritic Ca^{2+} spiking, we find that MLI-mediated inhibition shapes the induction of CF plasticity, affecting PF excitation of PCs. If activated in a coincident manner, MLIs

progressively negated the ability of CFs to produce associative plasticity at co-active PF synapses. Therefore, graded suppression of CF-mediated Ca^{2+} elevation supports the development of plasticity that opposes that induced by conjunctive PF and CF activity and resembles that produced by PF activation alone. As a result, activity-induced re-weighting of PF-evoked synaptic responses in PCs effectively obeys a Ca^{2+} threshold rule: directional alterations in PF response strength (Coesmans et al., 2004) occur across a continuous spectrum according to the level of MLI suppression of CF-evoked Ca^{2+} signaling in PCs.

Our results suggest that MLIs influence the induction of CF-mediated plasticity at two distinct sites: the first at the monosynaptic excitatory synaptic connections between PFs and PCs. MLI activation during the conjunctive CF stimulus converts CF-dependent LTD into non-associative LTP at this locus. The second plasticity site, at an unknown location, appears to affect the ability of MLIs to inhibit PCs. MLI-mediated feedforward inhibition is known to strongly temper the duration and amplitude of PF-evoked EPSPs (Mittmann et al., 2005). Our plasticity protocols consistently generated changes in PSP duration. This effect was absent when $GABA_A$ receptors were blocked, directly implicating an activity-induced alteration of MLI output. Also, alteration of MLI inhibitory strength seemed to contribute to determining the depth of PF-evoked PSP amplitude changes in PCs. Importantly, our results clearly show that plasticity at this second site was influenced by inhibitory regulation of CF-evoked PC dendritic Ca^{2+} signaling. Potentiation of PF-MLI synapses would promote the ability of PFs to drive feedforward inhibition, whereas PF-MLI depression would weaken it. Rebound potentiation (RP), a type of plasticity at MLI-PC synapses (Hirano et al., 2016), could also strengthen inhibition following CF activation. Due to its dependence on dendritic Ca^{2+} elevation in PCs (Kano et al., 1992, 1996), the induction of RP may be moderated when CF-evoked spiking occurs coincident with inhibition by MLIs.

MLI-Mediated Inhibition Can Produce Graded Learning

A prominent theory of cerebellar function posits that learning results from synaptic plasticity produced when CFs excite PCs in response to motor errors. During learning, if the CF-evoked dendritic Ca^{2+} signal in PCs is binary (i.e., all-or-none) then trial averaging is necessary to generate descriptive information about the error and generate plasticity proportional to the adjusted movement. This is an inefficient instructional coding scheme (Najafi and Medina, 2013). We find that optogenetic-induced MLI activity influences the magnitude and valence of CF-dependent motor adaptation. This suggests an alternative graded scheme generated by the inhibitory suppression of PC dendritic excitability and subsequent regulation of Ca^{2+}-dependent plasticity. In this way, inhibition from MLIs might effectively increase the capacity of CF instructive signaling, thereby allowing encoding of parametric information relevant to error-related variables (e.g., error magnitude), making learning more efficient (Najafi and Medina, 2013).

Whether a non-binary coding scheme is actually used by the cerebellum during CF-dependent learning will require additional investigation. However, in studies examining adaptive eye movements in monkeys, error magnitude is encoded by complex spike duration (Herzfeld et al., 2018; Yang and Lisberger, 2014). Short-duration complex spikes that correlate with less learning are, based on our findings, a hallmark of persistent MLI firing coincident with CF excitation. Direct recording of PC Ca^{2+} signals that instruct plasticity, rather than inference from complex spikes, will ultimately shed light on how CFs produce a range of learned behavior and how the amplitude of evoked PC Ca^{2+} responses relates to the activity level of MLIs. For the VOR, we expect that inhibition in association with ipsiversive head movements will regulate the magnitude of gain-increase learning during retinal slip errors because PC Ca^{2+} activity is susceptible to modulation by CF input during this phase of vestibular stimulation. Although MLIs in the vestibulo-cerebellum fire in a phase-specific manner, overlapping with the activity of CFs (Badura et al., 2013; Barmack and Yakhnitsa, 2008), there is a poor understanding of how the exact timing of the activity of these two inputs, and their firing rates, may change across different behavioral contexts.

MLI-Mediated Inhibition as a Gate for Learning Valence

Learned motor behavior necessarily must be bidirectional to accommodate either strengthening or weakening of movements during practice. For VOR adaptation, learning valence is thought to be differentially implemented through distinct types of plasticity (Boyden et al., 2004). How different forms of plasticity are generated in response to learning context is currently unresolved. Similar to previous reports (Kimpo et al., 2014; Nguyen-Vu et al., 2013), we found that activating CFs in association with ipsiversive head movements produced an increase in VOR gain, mimicking the behavioral response to opposite-direction visual-vestibular pairing. However, co-activation with MLIs progressively diminished the ability of CFs to induce gain-increase adaptation, culminating in a full reversal of learning valence with intensive optogenetic MLI stimulation, though the sensitivity of the switch in learning direction may depend on the timing of CF and MLI co-activity during vestibular motion. We conjecture that the switch in learning direction is mediated through the induction of opposite-sign plasticity, as observed in our acute slice recordings.

Gain-decrease learning resulting from same-direction visual-vestibular pairing modulates the activity of CFs during contraversive head turns (Ke et al., 2009). Yet contraversive optogenetic CF stimulation fails to induce learning (Kimpo et al., 2014; Nguyen-Vu et al., 2013). Interestingly, we found that CF optogenetic activation during contraversive head turns was ineffective at modulating PC Ca^{2+} activity. Gating of CF-evoked Ca^{2+} signaling by MLI activity with contraversive vestibular stimuli offers a plausible explanation for the inability of CFs to elicit gain adaptation during this context of head movement. As shown in our *ex vivo* recordings, inhibitory negation of CF-induced plasticity allows for PF-mediated strengthening of PSP amplitude. PF-PC LTP has been proposed to underlie gain-decrease learning (Boyden et al., 2004). Our hypothesis that MLI activity is responsible for enforcing gain-decrease adaptation by cancelling CF Ca^{2+} signaling in PCs is supported by our observation that optogenetic activation of MLIs had no additional influence on encoding this learned response (i.e., MLIs were already robustly active during this context). However, it is possible that gain-decrease learning is encoded outside of

the cerebellar cortex, apart from the activity of MLIs (Voges et al., 2017). Notably, mice with constitutive deletion of $GABA_A$ receptors from PCs can continue to adapt their VOR but are deficient in motor memory consolidation (Wulff et al., 2009). The influence of MLIs in this process therefore merits further study because long-term disruption of MLI signaling may result in compensatory circuit activity.

Together, our results support the theory that CF-dependent weakening of PF excitation of PCs contributes to gain-increase learning, whereas opposite-valence plasticity strengthens PF responses, resulting in gain-decrease learning (Boyden et al., 2004). That inhibition from MLIs facilitates a graded conversion of plasticity valence provides a circuit mechanism by which intermediate forms of motor learning may arise in a context-specific manner. This mechanism would also ensure that plasticity accurately corrects motor performance, as it would effectively gate the PC Ca^{2+} response to CF excitation. Thus, we conclude that, in cerebellar cortex as in other brain regions, inhibitory control of dendritic Ca^{2+} signaling and plasticity supports efficient learning and error correction to optimize motor performance.

STAR★METHODS

Detailed methods are provided in the online version of this paper and include the following:

- KEY RESOURCES TABLE
- CONTACT FOR REAGENT AND RESOURCE SHARING
- EXPERIMENTAL MODEL AND SUBJECT DETAILS
  - Animals
- METHOD DETAILS
  - Acute slice preparation
  - Electrophysiology
  - Two-photon imaging
  - Intracranial viral injections
  - Optical fiber and head-post implants
  - Optogenetic stimulation
  - Video-oculography and VOR training
  - Fiber Photometry
  - Histology and confocal imaging
- QUANTIFICATION AND STATISTICAL ANALYSIS

SUPPLEMENTAL INFORMATION

Supplemental Information includes nine figures and two tables and can be found with this article online at https://doi.org/10.1016/j.neuron.2018.07.024.

ACKNOWLEDGMENTS

We thank the members of the Christie Lab for their helpful discussion during the preparation of this manuscript. We are especially grateful for the efforts of Michael Gaffield and Himanshu Gangal for assistance with the development of data analysis software and Eric Patino for help with viral injections. We also thank the GENIE program and the Janelia Research Campus (Drs. Jayaraman, Kerr, Kim, Looger, and Svoboda) for use of GCaMP6f as well as Dr. Hirokazu Hirai (Gunma University, Japan) for assistance with the *L7* promoter in AAV. This work was supported by the Singapore Ministry of Education grant MOE2016-T2-1-097 (G.J.A.) as well as the Max Planck Society, the Max Planck Florida Institute for Neuroscience, and NIH grants NS083127 (M.J.M.R.) and NS083894 (J.M.C.).

AUTHOR CONTRIBUTIONS

Conceptualization, M.J.M.R., A.B., and J.M.C.; Methodology, M.J.M.R., A.B., and J.M.C.; Resources, C.K., G.J.A., and H.T.; Investigation, M.J.M.R., A.B., K.Z., and S.B.A.; Writing, J.M.C.; Editing, M.J.M.R., G.J.A., and J.M.C.; Funding Acquisition, M.J.M.R. and J.M.C.; Supervision, J.M.C.

DECLARATION OF INTERESTS

The authors declare no competing interests.

Received: December 18, 2017
Revised: June 6, 2018
Accepted: July 17, 2018
Published: August 16, 2018

REFERENCES

Amat, S.B., Rowan, M.J.M., Gaffield, M.A., Bonnan, A., Kikuchi, C., Taniguchi, H., and Christie, J.M. (2017). Using c-kit to genetically target cerebellar molecular layer interneurons in adult mice. PLoS ONE *12*, e0179347.

Badura, A., Schonewille, M., Voges, K., Galliano, E., Renier, N., Gao, Z., Witter, L., Hoebeek, F.E., Chédotal, A., and De Zeeuw, C.I. (2013). Climbing fiber input shapes reciprocity of Purkinje cell firing. Neuron *78*, 700–713.

Barmack, N.H., and Yakhnitsa, V. (2008). Functions of interneurons in mouse cerebellum. J. Neurosci. *28*, 1140–1152.

Boyden, E.S., and Raymond, J.L. (2003). Active reversal of motor memories reveals rules governing memory encoding. Neuron *39*, 1031–1042.

Boyden, E.S., Katoh, A., and Raymond, J.L. (2004). Cerebellum-dependent learning: the role of multiple plasticity mechanisms. Annu. Rev. Neurosci. *27*, 581–609.

Callaway, J.C., Lasser-Ross, N., and Ross, W.N. (1995). IPSPs strongly inhibit climbing fiber-activated [Ca2+]i increases in the dendrites of cerebellar Purkinje neurons. J. Neurosci. *15*, 2777–2787.

Carey, M.R., Medina, J.F., and Lisberger, S.G. (2005). Instructive signals for motor learning from visual cortical area MT. Nat. Neurosci. *8*, 813–819.

Chen, T.W., Wardill, T.J., Sun, Y., Pulver, S.R., Renninger, S.L., Baohan, A., Schreiter, E.R., Kerr, R.A., Orger, M.B., Jayaraman, V., et al. (2013). Ultrasensitive fluorescent proteins for imaging neuronal activity. Nature *499*, 295–300.

Chen, S., Augustine, G.J., and Chadderton, P. (2017). Serial processing of kinematic signals by cerebellar circuitry during voluntary whisking. Nat. Commun. *8*, 232.

Chiu, C.Q., Lur, G., Morse, T.M., Carnevale, N.T., Ellis-Davies, G.C., and Higley, M.J. (2013). Compartmentalization of GABAergic inhibition by dendritic spines. Science *340*, 759–762.

Coddington, L.T., Rudolph, S., Vande Lune, P., Overstreet-Wadiche, L., and Wadiche, J.I. (2013). Spillover-mediated feedforward inhibition functionally segregates interneuron activity. Neuron *78*, 1050–1062.

Coesmans, M., Weber, J.T., De Zeeuw, C.I., and Hansel, C. (2004). Bidirectional parallel fiber plasticity in the cerebellum under climbing fiber control. Neuron *44*, 691–700.

Davie, J.T., Clark, B.A., and Häusser, M. (2008). The origin of the complex spike in cerebellar Purkinje cells. J. Neurosci. *28*, 7599–7609.

Dittman, J.S., and Regehr, W.G. (1998). Calcium dependence and recovery kinetics of presynaptic depression at the climbing fiber to Purkinje cell synapse. J. Neurosci. *18*, 6147–6162.

Dizon, M.J., and Khodakhah, K. (2011). The role of interneurons in shaping Purkinje cell responses in the cerebellar cortex. J. Neurosci. *31*, 10463–10473.

Eccles, J.C., Llinás, R., and Sasaki, K. (1966). The excitatory synaptic action of climbing fibres on the Purkinje cells of the cerebellum. J. Physiol. *182*, 268–296.

Finch, E.A., Tanaka, K., and Augustine, G.J. (2012). Calcium as a trigger for cerebellar long-term synaptic depression. Cerebellum *11*, 706–717.

Gaffield, M.A., and Christie, J.M. (2017). Movement rate is encoded and influenced by widespread, coherent activity of cerebellar molecular layer interneurons. J. Neurosci. *37*, 4751–4765.

Gaffield, M.A., Amat, S.B., Bito, H., and Christie, J.M. (2016). Chronic imaging of movement-related Purkinje cell calcium activity in awake behaving mice. J. Neurophysiol. *115*, 413–422.

Hashimoto, K., and Kano, M. (1998). Presynaptic origin of paired-pulse depression at climbing fibre-Purkinje cell synapses in the rat cerebellum. J. Physiol. *506*, 391–405.

Häusser, M., and Clark, B.A. (1997). Tonic synaptic inhibition modulates neuronal output pattern and spatiotemporal synaptic integration. Neuron *19*, 665–678.

Herzfeld, D.J., Kojima, Y., Soetedjo, R., and Shadmehr, R. (2018). Encoding of error and learning to correct that error by the Purkinje cells of the cerebellum. Nat. Neurosci. *21*, 736–743.

Hirano, T., Yamazaki, Y., and Nakamura, Y. (2016). LTD, RP, and motor learning. Cerebellum *15*, 51–53.

Ito, M. (1972). Neural design of the cerebellar motor control system. Brain Res. *40*, 81–84.

Ito, M. (1982). Cerebellar control of the vestibulo-ocular reflex–around the flocculus hypothesis. Annu. Rev. Neurosci. *5*, 275–296.

Ito, M., and Kano, M. (1982). Long-lasting depression of parallel fiber-Purkinje cell transmission induced by conjunctive stimulation of parallel fibers and climbing fibers in the cerebellar cortex. Neurosci. Lett. *33*, 253–258.

Jelitai, M., Puggioni, P., Ishikawa, T., Rinaldi, A., and Duguid, I. (2016). Dendritic excitation-inhibition balance shapes cerebellar output during motor behaviour. Nat. Commun. *7*, 13722.

Jörntell, H., and Ekerot, C.F. (2002). Reciprocal bidirectional plasticity of parallel fiber receptive fields in cerebellar Purkinje cells and their afferent interneurons. Neuron *34*, 797–806.

Jörntell, H., and Ekerot, C.F. (2003). Receptive field plasticity profoundly alters the cutaneous parallel fiber synaptic input to cerebellar interneurons in vivo. J. Neurosci. *23*, 9620–9631.

Kano, M., Rexhausen, U., Dreessen, J., and Konnerth, A. (1992). Synaptic excitation produces a long-lasting rebound potentiation of inhibitory synaptic signals in cerebellar Purkinje cells. Nature *356*, 601–604.

Kano, M., Kano, M., Fukunaga, K., and Konnerth, A. (1996). Ca(2+)-induced rebound potentiation of gamma-aminobutyric acid-mediated currents requires activation of Ca2+/calmodulin-dependent kinase II. Proc. Natl. Acad. Sci. USA *93*, 13351–13356.

Ke, M.C., Guo, C.C., and Raymond, J.L. (2009). Elimination of climbing fiber instructive signals during motor learning. Nat. Neurosci. *12*, 1171–1179.

Kim, J., Lee, S., Tsuda, S., Zhang, X., Asrican, B., Gloss, B., Feng, G., and Augustine, G.J. (2014). Optogenetic mapping of cerebellar inhibitory circuitry reveals spatially biased coordination of interneurons via electrical synapses. Cell Rep. *7*, 1601–1613.

Kim, C.K., Yang, S.J., Pichamoorthy, N., Young, N.P., Kauvar, I., Jennings, J.H., Lerner, T.N., Berndt, A., Lee, S.Y., Ramakrishnan, C., et al. (2016). Simultaneous fast measurement of circuit dynamics at multiple sites across the mammalian brain. Nat. Methods *13*, 325–328.

Kimpo, R.R., Rinaldi, J.M., Kim, C.K., Payne, H.L., and Raymond, J.L. (2014). Gating of neural error signals during motor learning. eLife *3*, e02076.

Kitamura, K., and Häusser, M. (2011). Dendritic calcium signaling triggered by spontaneous and sensory-evoked climbing fiber input to cerebellar Purkinje cells in vivo. J. Neurosci. *31*, 10847–10858.

Konnerth, A., Dreessen, J., and Augustine, G.J. (1992). Brief dendritic calcium signals initiate long-lasting synaptic depression in cerebellar Purkinje cells. Proc. Natl. Acad. Sci. USA *89*, 7051–7055.

Lamont, M.G., and Weber, J.T. (2012). The role of calcium in synaptic plasticity and motor learning in the cerebellar cortex. Neurosci. Biobehav. Rev. *36*, 1153–1162.

Lee, K.H., Mathews, P.J., Reeves, A.M., Choe, K.Y., Jami, S.A., Serrano, R.E., and Otis, T.S. (2015). Circuit mechanisms underlying motor memory formation in the cerebellum. Neuron *86*, 529–540.

Lev-Ram, V., Wong, S.T., Storm, D.R., and Tsien, R.Y. (2002). A new form of cerebellar long-term potentiation is postsynaptic and depends on nitric oxide but not cAMP. Proc. Natl. Acad. Sci. USA *99*, 8389–8393.

Linden, D.J., and Connor, J.A. (1995). Long-term synaptic depression. Annu. Rev. Neurosci. *18*, 319–357.

Mathews, P.J., Lee, K.H., Peng, Z., Houser, C.R., and Otis, T.S. (2012). Effects of climbing fiber driven inhibition on Purkinje neuron spiking. J. Neurosci. *32*, 17988–17997.

Medina, J.F. (2011). The multiple roles of Purkinje cells in sensori-motor calibration: to predict, teach and command. Curr. Opin. Neurobiol. *21*, 616–622.

Medina, J.F., Repa, J.C., Mauk, M.D., and LeDoux, J.E. (2002). Parallels between cerebellum- and amygdala-dependent conditioning. Nat. Rev. Neurosci. *3*, 122–131.

Mittmann, W., and Häusser, M. (2007). Linking synaptic plasticity and spike output at excitatory and inhibitory synapses onto cerebellar Purkinje cells. J. Neurosci. *27*, 5559–5570.

Mittmann, W., Koch, U., and Häusser, M. (2005). Feed-forward inhibition shapes the spike output of cerebellar Purkinje cells. J. Physiol. *563*, 369–378.

Najafi, F., and Medina, J.F. (2013). Beyond "all-or-nothing" climbing fibers: graded representation of teaching signals in Purkinje cells. Front. Neural Circuits *7*, 115.

Najafi, F., Giovannucci, A., Wang, S.S., and Medina, J.F. (2014a). Coding of stimulus strength via analog calcium signals in Purkinje cell dendrites of awake mice. eLife *3*, e03663.

Najafi, F., Giovannucci, A., Wang, S.S., and Medina, J.F. (2014b). Sensory-driven enhancement of calcium signals in individual Purkinje cell dendrites of awake mice. Cell Rep. *6*, 792–798.

Nguyen-Vu, T.D., Kimpo, R.R., Rinaldi, J.M., Kohli, A., Zeng, H., Deisseroth, K., and Raymond, J.L. (2013). Cerebellar Purkinje cell activity drives motor learning. Nat. Neurosci. *16*, 1734–1736.

Nitta, K., Matsuzaki, Y., Konno, A., and Hirai, H. (2017). Minimal Purkinje cell-specific PCP2/L7 promoter virally available for rodents and non-human primates. Mol. Ther. Methods Clin. Dev. *6*, 159–170.

Otsu, Y., Marcaggi, P., Feltz, A., Isope, P., Kollo, M., Nusser, Z., Mathieu, B., Kano, M., Tsujita, M., Sakimura, K., and Dieudonné, S. (2014). Activity-dependent gating of calcium spikes by A-type K+ channels controls climbing fiber signaling in Purkinje cell dendrites. Neuron *84*, 137–151.

Ozden, I., Dombeck, D.A., Hoogland, T.M., Tank, D.W., and Wang, S.S. (2012). Widespread state-dependent shifts in cerebellar activity in locomoting mice. PLoS ONE *7*, e42650.

Piochon, C., Titley, H.K., Simmons, D.H., Grasselli, G., Elgersma, Y., and Hansel, C. (2016). Calcium threshold shift enables frequency-independent control of plasticity by an instructive signal. Proc. Natl. Acad. Sci. USA *113*, 13221–13226.

Rajasethupathy, P., Sankaran, S., Marshel, J.H., Kim, C.K., Ferenczi, E., Lee, S.Y., Berndt, A., Ramakrishnan, C., Jaffe, A., Lo, M., et al. (2015). Projections from neocortex mediate top-down control of memory retrieval. Nature *526*, 653–659.

Rancillac, A., and Crépel, F. (2004). Synapses between parallel fibres and stellate cells express long-term changes in synaptic efficacy in rat cerebellum. J. Physiol. *554*, 707–720.

Rancz, E.A., and Häusser, M. (2006). Dendritic calcium spikes are tunable triggers of cannabinoid release and short-term synaptic plasticity in cerebellar Purkinje neurons. J. Neurosci. *26*, 5428–5437.

Raymond, J.L., and Lisberger, S.G. (1998). Neural learning rules for the vestibulo-ocular reflex. J. Neurosci. *18*, 9112–9129.

Schultz, W., and Dickinson, A. (2000). Neuronal coding of prediction errors. Annu. Rev. Neurosci. *23*, 473–500.

Stahl, J.S. (2004). Eye movements of the murine P/Q calcium channel mutant rocker, and the impact of aging. J. Neurophysiol. *91*, 2066–2078.

Stahl, J.S., van Alphen, A.M., and De Zeeuw, C.I. (2000). A comparison of video and magnetic search coil recordings of mouse eye movements. J. Neurosci. Methods *99*, 101–110.

Suvrathan, A., Payne, H.L., and Raymond, J.L. (2016). Timing rules for synaptic plasticity matched to behavioral function. Neuron *92*, 959–967.

Szapiro, G., and Barbour, B. (2007). Multiple climbing fibers signal to molecular layer interneurons exclusively via glutamate spillover. Nat. Neurosci. *10*, 735–742.

Tanaka, K., Khiroug, L., Santamaria, F., Doi, T., Ogasawara, H., Ellis-Davies, G.C., Kawato, M., and Augustine, G.J. (2007). Ca^{2+} requirements for cerebellar long-term synaptic depression: role for a postsynaptic leaky integrator. Neuron *54*, 787–800.

ten Brinke, M.M., Boele, H.J., Spanke, J.K., Potters, J.W., Kornysheva, K., Wulff, P., IJpelaar, A.C., Koekkoek, S.K., and De Zeeuw, C.I. (2015). Evolving models of Pavlovian conditioning: cerebellar cortical dynamics in awake behaving mice. Cell Rep. *13*, 1977–1988.

Voges, K., Wu, B., Post, L., Schonewille, M., and De Zeeuw, C.I. (2017). Mechanisms underlying vestibulo-cerebellar motor learning in mice depend on movement direction. J. Physiol. *595*, 5301–5326.

Wang, S.S., Denk, W., and Häusser, M. (2000). Coincidence detection in single dendritic spines mediated by calcium release. Nat. Neurosci. *3*, 1266–1273.

Wulff, P., Schonewille, M., Renzi, M., Viltono, L., Sassoè-Pognetto, M., Badura, A., Gao, Z., Hoebeek, F.E., van Dorp, S., Wisden, W., et al. (2009). Synaptic inhibition of Purkinje cells mediates consolidation of vestibulo-cerebellar motor learning. Nat. Neurosci. *12*, 1042–1049.

Yang, Y., and Lisberger, S.G. (2014). Purkinje-cell plasticity and cerebellar motor learning are graded by complex-spike duration. Nature *510*, 529–532.

STAR★METHODS

KEY RESOURCES TABLE

REAGENT or RESOURCE	SOURCE	IDENTIFIER
Antibodies		
Rabbit polyclonal anti-Calbindin	Swant	Cat# CB38a; RRID: AB_10000340
Mouse monoclonal anti-VGLUT2	Abcam	Cat# ab579157; RRID: AB_1603114
AlexaFluor 633 goat anti-rabbit	Thermo Fisher Scientific	Cat# A-21070; RRID: AB_2535731
AlexaFluor 633 goat anti-mouse	Thermo Fisher Scientific	Cat# A-21072; RRID: AB_2535733
Bacterial and Virus Strains		
AAV1-EF1α-Flex(*loxP*)-ChR2(H134R)-YFP	Penn Vector Core	Cat# AV-1-20298P
AAV5-EF1α-Flex(*loxP*)-bReaChES-EYFP	UNC Vector Core	N/A
AAV5-αCaMKII-bReaChES-EYFP	UNC Vector Core	N/A
AAV1-αCaMKII-GFP	Penn Vector Core	Cat# AV-1-PV1917
AAV1-CAG- Flex(*loxP*)-GFP	UNC Vector Core	N/A
AAV1-L7.6-FlpO	Custom Prep (ViGene)	N/A
AAV1-Flex(FRT)-GCaMP6f	Custom Prep (ViGene)	N/A
Chemicals, Peptides, and Recombinant Proteins		
Alexa 594	Life Technologies	Cat# A10438
Fluo-5F	Life Technologies	Cat# F14221
NBQX	Tocris	Cat# 0373
(R)-CPP	Tocris	Cat# 0247
SR 95531	Tocris	Cat# 1262
CGP 35348	Tocris	Cat# 1245
Experimental Models: Organisms/Strains		
Mouse: C57BL/6J	The Jackson Laboratory	Stock# 000664; RRID: IMSR_JAX:000664
Mouse: nNOS-ChR2	Kim et al., 2014	N/A
Mouse: *c-kit::Cre*	Amat et al., 2017	N/A
Software and Algorithms		
Axograph X	Axograph	https://www.axograph.com; RRID: SCR_014284
GraphPad Prism	Graphpad software	https://www.graphpad.com; RRID: SCR_002798
ImageJ	NIH	http://fiji.sc; RRID: SCR_003070
ISCAN ETL-200	ISCAN	http://www.iscan.com
PsychoPy	Psychopy.org	http://www.psychopy.org; RRID: SCR_006571
MATLAB	MathWorks	https://www.mathworks.com; RRID: SCR_001622
pClamp 10 (Clampex)	Molecular Devices	RRID: SCR_011323
LabView	National Instruments	RRID: SCR_014325

CONTACT FOR REAGENT AND RESOURCE SHARING

Requests for resources and reagents should be directed to the Lead Contact, Jason Christie (jason.christie@mpfi.org), and will be fulfilled in a timely manner.

EXPERIMENTAL MODEL AND SUBJECT DETAILS

Animals

Mice used in this study included animals from wild-type (Wt), heterozygous nNos-ChR2 and heterozygous *c-kit::Cre* lines, all maintained on a C57BL/6J background. Experiments were performed on mature animals *(ex vivo* physiology: mean = 8 weeks; range = 6

to 15 weeks; *in vivo* behavior: mean = 15 weeks; range = 8 to 23 weeks) of either sex. All animal procedures used in this study were approved by the Max Planck Florida Institute for Neuroscience Animal Care and Use Committee (IACUC).

METHOD DETAILS

Acute slice preparation

Under ketamine/xylazine anesthesia (intraperitoneal injection; 20mg/ml; 2mg/ml respectively), mice were transcardially perfused with cold saline (~4°C) to rapidly chill the brain. Immediately following, the cerebellum was removed by dissection. From this tissue, slices (200 μm) were sectioned in the parasagittal orientation from the lateral cortical hemisphere or the floccular complex using a vibrating blade microtome (VT1200S, Leica Biosystems) in an icy solution containing (in mM) 87 NaCl, 25 $NaHO_3$, 2.5 KCl, 1.25 NaH_2PO_4, 7 $MgCl_2$, 0.5 $CaCl_2$, 10 glucose, and 75 sucrose. Slices from either location were used for dendritic recordings, but only floccular/parafloccular slices were used for long-term plasticity experiments. Slices were transferred to an incubation chamber containing a similar solution but with (in mM) 128 NaCl, 26.2 $NaHO_3$, 2.5 KCl, 1 NaH_2PO_4, 1.5 $CaCl_2$, 1.5$MgCl_2$ and 11 glucose and maintained at 34°C for 40 min and then at room temperature (23-25°C) thereafter. During whole-cell recording, slices were continuously perfused with the same solution warmed to 34°C with an inline heater (TC-344; Warner Instruments). All solutions were equilibrated and maintained with carbogen gas (95% O_2/5% CO_2). Where noted, inhibitory synaptic transmission was blocked pharmacologically with 20 μM SR 95531 (Tocris) while excitatory transmission was blocked with 20 μM NBQX and 20 μM (R)-CPP (Tocris).

Electrophysiology

Neurons were targeted for somatic whole-cell recording using gradient-contrast video-microscopy. PCs were identified by their characteristic morphology. MLIs were identified by their location in the molecular layer. We did not discriminate between stellate and basket cells in our recordings. Granule cells and Golgi cells were identified based on their location in the granule layer and by their distinct electrophysiological characteristics (Golgi cell capacitance ~30 pF; granule cell capacitance ~5 pF). PC dendrites and axons were patched in the whole-cell or cell-attached patch configuration, respectively, using a fluorescence-guided technique. In this approach, pipettes were fluorescently coated by briefly dipping the glass electrodes in BSA-conjugated Alexa Fluor-594 (Life Technologies; 0.02% w/v in 100 μM BSA) and, after drying (< 5 min), were filled with intracellular solution and immediately used for recording. For both somatic and dendritic whole-cell recording, borosilicate patch pipettes contained an intracellular solution composed of (in mM) 124 potassium gluconate, 2 KCl, 9 HEPES, 4 $MgCl_2$, 4 NaATP, 3 L-Ascorbic Acid, and 0.5 NaGTP (pH = 7.25). Open tip resistance was 2-5 MΩ and 2-6 MΩ for somatic and dendritic patch pipettes, respectively. For axons, loose-seal recordings (~30 MΩ) were obtained with 10-15 MΩ pipettes containing (in mM) 119 NaCl, 2.5 KCl, 12 HEPES, 17 Dextrose, and 3 $MgCl_2$ (pH = 7.25). During whole-cell recording, constant current injection maintained the membrane potential of PCs at a near-threshold level (~-50 mV) except for plasticity experiments where the membrane potential was maintained at a more hyperpolarized potential (~-80 mV) to prevent PF-evoked PSPs from eliciting Na^+ spikes. The membrane potential of MLIs was maintained at −70 mV during recording from this cell type.

Electrophysiological measurements were obtained using Multiclamp 700B amplifiers (Molecular Devices). Analog signals were filtered at 2-10 kHz and sampled at 20-50 kHz using a Digidata 1440 digitizer (Molecular Devices). Data was collected on a Windows PC using pClamp 10 software (Molecular Devices). Pipette capacitance was neutralized in all recordings and electrode series resistance compensated using bridge balance in current-clamp mode. Liquid junctional potentials, determined to be −10 mV, were corrected for in our recordings. Brief electrical pulses (100 μs; 1 - 5 V) applied through a constant voltage stimulus isolation unit (Model DS2A; Digitimer) were used to activate CFs with bi-polar glass pipettes placed near the PC layer. PFs were stimulated electrically with a glass pipette placed in the molecular layer in the vicinity of the PC dendritic arbor.

CF stimulation evoked dendritic Ca^{2+} spikes which were identified as sharp increases in the first derivative of the trial-averaged waveform. The timing of spike onset was determined at the 10% rise point of the first derivative, which was used to determine the baseline epoch for each spike when measuring peak amplitudes of Ca^{2+} spikes in the voltage trace. Our estimates of average MLI firing rate elicited by optogenetic activation, determined in separate calibration experiments, did not account for spontaneous firing in these cells in the absence of direct stimulation. For long-term plasticity experiments, test responses to PF stimulation were elicited at 0.066 Hz and were averaged (4 trials per point) in the plots of peak amplitude over time. For the ANOVA analysis, the average baseline response (10 min; 40 trials) was compared to the average response between 35-45 minutes (40 trials). To quantify PSP kinetics, waveforms were fit with a mono-exponential decay function (τ). Average changes in τ were calculated before (10 minutes) and after (30-40 minutes) induction protocols and normalized to baseline for comparison.

Two-photon imaging

PCs were imaged in acute cerebellar slices with a two-photon laser scanning microscope (2pLSM) using a commercial scan head (Ultima; Bruker Corp) fitted with galvanometer mirrors (Cambridge Technology). The scan head sat on an Olympus upright microscope (BX51WI) using an objective (60x, 1.0 NA) and oil immersion condenser (1.4 NA). 2p excitation (λ = 810 nm) was provided

by a mode-locking Ti:sapphire laser (Chameleon Ultra II; Coherent). Fluorescence emission was detected using GaAsP photomultiplier modules (Hamamatsu) with a t560lpxr dichroic and et640/120-2p and et510/80-2p bandpass filters (Chroma) for chromatic separation.

For fluorescence-guided patching, continuous 2pLSM imaging was used to visually guide dye-coated pipettes to the dye-labeled neurites of PCs filled somatically with the morphological indicator Alexa 594 (60 μM; Life Technologies). For Ca^{2+} imaging, PCs were filled through the whole-cell pipette with the green Ca^{2+} indicator Fluo-5F (200 μM) as well as the red-volume indicator Alexa 594 (60 μM) to identify their dendritic processes. Spiny dendritic shafts or individual spines were selected for imaging. Red fluorescence from the volumetric dye was not collected during functional imaging because amber light used for photo-activation of bReaChES ($\lambda = \sim$590 nm) would damage the PMT used for detecting emission of the red fluorophore. Therefore, Ca^{2+} changes were quantified using $\Delta F/F$ rather than $\Delta G/R$. To determine the amplitude of the CF-evoked Ca^{2+} response in the PC dendrite, we used an exponential fit to the decay of the elicited transient measuring the peak of this fit at the time point immediately after cessation of the optogenetic stimulus. In this analysis, the optogenetic stimulus artifact was blanked for quantification. A corresponding epoch of time in the control response was also blanked to facilitate comparison between conditions.

Intracranial viral injections

To optogenetically activate MLIs, *c-kit::Cre* mice were injected with AAV1-EF1α-Flex(*loxP*)-ChR2(H134R)-YFP or AAV5-EF1α-Flex(*loxP*)-bReaChES-EYFP in the lateral hemispheres (targeting lobules Crus I and II) or the flocculi. To optogenetically activate CFs, AAV5-αCaMKIIa-bReachES-EYFP was injected in the inferior olive of both WT and nNOS-ChR2 mice. For control experiments, AAV1-αCaMKIIa-GFP and AAV1-CAG-Flex(*loxP*)-GFP were injected in the inferior olive and flocculi of *c-kit::Cre* mice, respectively. This was in place of viruses containing light-sensitive opsins. To measure *in vivo* Ca^{2+} activity in PCs, we used a virus strategy leveraging the activity of the *L7/Pcp2* promoter, AAV1- L7.6-FlpO, to drive FlpO recombinase expression specifically in PCs of WT mice (Nitta et al., 2017). A second FlpO-dependent virus, AAV1- CAG-Flex(FRT)-GCaMP6f, was co-injected to allow for high-level expression of the genetically encoded Ca^{2+} indicator in transduced floccular PCs. These mice were also injected in the IO with AAV5-αCaMKIIa-bReachES-EYFP to stimulate CFs. AAVs were obtained from vector core facilities of either the University of Pennsylvania or University of North Carolina, or custom packaged at ViGene (Rockville, MD).

When performing viral injections, mice were held by head-fixation in a stereotactic platform (David Kopf Instruments) using ear bars, while under isoflurane anesthesia (1.8 - 4.0%). Thermoregulation was provided by a heating plate using a rectal thermocouple for biofeedback, thus maintaining core body temperature near 37°C. During anesthesia, the eyes were protected with ophthalmic ointment. A lidocaine/bupivacaine cocktail was subcutaneously injected into the scalp to induce local anesthesia. A small incision was opened (< 2 mm) above the cerebellum and a craniotomy was cut in the skull (< 0.5 μm in diameter) to allow access for the glass microinjection pipette. Coordinates (in mm from Bregma) for microinjection were X = ± 3.10 −3.50; Y = −2.1; α = 0°; Z = 0.25 - 1.00 for targeting the lateral hemispheres and X = ± 2.33; Y = −5.68; α = 10°; Z = 3.2 - 3.4 for targeting the flocculi. For IO injections, the glass micropipette was inserted through the exposed dura mater between the foramen magnum and C1 vertebra at a 62° vertical angle. Bilateral injections were made at 2.6 - 2.7 mm in depth and 0.24 - 0.30 mm from midline.

Undiluted viral solution (titer ≥ 10^{12} vg/mL) was injected slowly (~0.05 - 0.1 μL min^{-1}) by pressure (0.2 - 0.5 μL per site). After ejection of virus, the micropipette was held in place (5 - 10 min) before withdrawal. The scalp was closed with surgical sutures or gluture and the animal was allowed to recover under analgesia provided by injection of carprofen and buprenorphine SR LAB (5 mg/kg and 0.35 mg/kg, respectively). After allowing for onset of expression (10 - 21 days), animals were either sacrificed and brains harvested for preparation of acute slices, or were used for behavior experimentation.

Optical fiber and head-post implants

After recovery from the viral injection surgery (≥7 days), mice used for behavioral experiments were implanted with head-posts for restraint as well as optical fibers to deliver laser light to the cerebellum. Animals were again placed in a stereotactic platform under isoflurane anesthesia (1.8 - 4.0%) using a heating pad to maintain normal body temperature. After subcutaneous injection of local anesthetics (lidocaine/bupivacaine), a large portion of the skull was exposed through surgical excision of the scalp. Custom-made optical fibers (200 μm, NA 0.22 with Ø 1.25 mm ferrules; Thorlabs) were bilaterally implanted in each side of the cerebellum targeting each flocculus (coordinates X = ± 3.35 mm; Y = 5.65 mm; α = −16°; *z* = 1.9 ± 0.1 mm); a unilateral implant was used for photometry (MFC_400/430-0.48_MF1.25_FLT, Doric Lenses) targeting a similar location (X = 2.35 mm; Y = 5.65 mm; α = 10°; z = 3 ± 0.1 mm). Optical fibers were secured to the skull using dental cement onto dry bone. Finally, a custom-engineered stainless steel head-post was attached to the skull with dental cement (Metabond; Parkell) centered on the midline of the cranium. The appropriate location of the optical fibers was confirmed prior to experiments by the ability to induce eye movements to high-intensity optogenetic stimuli in quiescence as well as after completion of experiments by post hoc examination of aldehyde-perfused tissue.

Optogenetic stimulation

During *ex vivo* optogenetic slice experiments, ChR2 was excited using blue light from an unfiltered LED (M470L3; Thorlabs) centered on λ = 461 nm (±20 nm). When exciting bReaChES, an unfiltered amber LED (M590L3; Thorlabs) centered on λ = 596 nm (±15 nm) was used instead. Light from the blue and amber LEDs was combined using a dichroic (T570plxr; Chroma) launched through the rear epiport of the microscope, and then reflected into the back of objective using a second dichroic (700dcxru; Chroma), which also allowed

for the transmission of 2p excitation laser light though a separate pathway. LEDs were rapidly modulated (< 1 kHz) with a specialized current controller (LEDD1B; Thorlabs) triggered by TTL commands produced by the electrophysiology software.

During *in vivo* optogenetic experiments, a blue-light emitting DPSS laser was used to activate ChR2 (CNI Optoelectronics Tech; MBL-F-473-200mW) centered on 473 nm (±1 nm) with a separate DPSS laser providing amber light centered on 589 nm (±1 nm) to activate bReaChES (CNI Optoelectronics Tech; MGL-F-589-200mW). After a shutter (NS15B1T0-ED; Vincent Associates), light from each laser source was split into two lines using a wave plate (WPH05M-473 and WPH05M-588, for blue and amber light, respectively; Thorlabs) and beamsplitter cube (PBS101; Thorlabs). Each line was directed through an AOM (AA Opto-Electronic; MTS110-A3-VIS) allowing for the rapid (< 1 kHz), independent modulation of laser power of either line for both wavelengths of light. From each AOM, laser light was launched into fiber ports (PAF-X-11-A; Thorlabs). Separate blue and amber lines were combined using a fiber-compatible dichroic mirror mount (Mini-cube E[470]_E[590]; Doric Lenses). Using patch cables (MFP_200/240/900-0.22; Doric Lenses), dual-color light stimuli could be delivered to fiber implants targeting both flocculi.

The stimulus conditions for activating CFs *in vivo* were guided by observations from our *ex-vivo* slice experiments. The efficacy of optogenetic stimuli to excite CFs was validated using PC Ca^{2+} activity monitoring. Likewise, the conditions for dual-color optogenetic stimulation were informed by our observations from slice experiments. The duration of the MLI stimulus was the approximate duration of the CF-evoked burst Ca^{2+} spikes in the PC dendrite. We increased the duration of this stimulus for coincident activation with CFs *in vivo* (from 20 ms to 25 ms) to account for the slight delay in evoking a complex spike in PCs after bReaChES-induced CF excitation (approx. 5 ms). The ability to activate MLIs by ChR2 stimulation was confirmed *in vivo* by optogenetic-induced eye movements in response to blue light stimuli in nNOS-ChR2 and AAV-injected *c-kit::Cre* mice. Evaluating a range of test stimuli in quiescent mice, we selected an illumination power just below threshold for eliciting a short latency contribution to the VOR-evoked eye movement in that mouse. We used half this power when examining for a graded influence of MLI activity on gain-increase VOR adaption. The duration and timing of optogenetic stimuli for MLI activation during visual-vestibular pairing experiments corresponded approximately to the period of VOR-evoked Ca^{2+} activity in PCs, measured in separate experiments using photometry.

Video-oculography and VOR training

Mice were head-restrained using their surgically implanted head-posts on a custom-made VOR apparatus. The apparatus was fully enclosed for light control. The apparatus included a motorized rotation stage (T-RSW60C, Zaber Technology) to deliver horizontal vestibular stimuli. A high-accuracy quadrature encoder (IT3402C; Posic) was used to monitor stage position. Mice were secured on the apparatus with their left eye at the center of the stage. A CCD camera outfitted with a high-magnification, machine-vision lens (MVL6X12Z; Thorlabs) was directed at the eye. The camera was attached to the apparatus by a rail on the perimeter of stage allowing translation of its position equidistant from the center of the eye. Once secured, the camera allowed for non-invasive monitoring of eye position. Relative eye movements were computed by tracking the pupil with a commercial video system (ETL-200; ISCAN). Using a propriety algorithm, the eye-tracking system calculated horizontal pupil position (120 Hz) as well as pupil diameter, outputting this information as linearized voltage signals. Three infrared (IR) LEDs were used to illuminate the eye. Two LEDs, fixed to the rotation stage, were positioned below the eye. A third LED (M940L3; Thorlabs) was fixed to the top of the camera to provide IR illumination as well as a reference corneal reflection (*CR*) used for analysis procedures. Two LCD monitors placed on either side of the apparatus were used to provide visual stimuli. Solid-state relays toggled power to the LED backlights of the monitors so that they could be rapidly rendered completely dark by a TTL command. DAQ boards (PXIe-6356 and PXIe-6383; National Instruments) allowed for interfacing with a computer providing user control of both the VOR apparatus and lasers for optogenetic stimulation as well as recording stage position, eye metrics (from the voltage outputs of the eye-tracking system), laser commands, and visual stimuli. Control was implemented through custom-written software written in LabVIEW (National Instruments).

The angular position of the eye was derived using a previously published method (Stahl et al., 2000). This included a calibration procedure for each animal prior to each experiment to estimate the distance of the plane of the pupil to the center of the corneal curvature, i.e., the radius of pupil rotation (*Rp*). For the *Rp* calibration, the camera was translated back-and-forth on the rail around the vertical axis of the stage with a known angle (±10°). The measured pupil position (*P*) was corrected for motion-induced artifacts by subtracting the corresponding *CR* position. Calibration measurements were made for several different pupil diameters to accommodate for a range of diameters encountered during an experiment. Pupil diameter was altered by changing the illumination intensity of a white-light emitting LED flood lamp. *Rp* was calculated across pupil diameters according to: $Rp = \Delta/\sin(20^\circ)$. By selecting *Rp* values in accordance with pupil diameter changes over the course of an experiment, angular eye position was determined throughout an experiment by the following formula: $Eye\ position\ (Ep) = \arcsin[(P_1\text{-}CR_1)\text{-}(P_2\text{-}CR_2)/Rp]$. VOR performance was determined from eye movements evoked by head rotation in the absence of light. Prior to experiments, pilocarpine (2% ophthalmic drops; Patterson Veterinary Supply) was briefly applied (< 1 min) onto the eye to limit pupil dilatation so that the eye could be accurately tracked in darkness. VOR gain was calculated as the amplitude ratio between eye velocity and stage velocity. One day prior to the start of training procedures, mice were familiarized with the VOR apparatus for ~15 min. This increased their comfort level improving the quality of eye-tracking.

To instruct artificial VOR adaptation using dual-color optogenetics, mice were trained with photo-activation of CFs and/or MLIs while being passively rotated in darkness. The absence of light prevented the mice from experiencing visual information that could help guide learning. Sinusoidal stage movements were used for vestibular stimuli; laser pulses for optogenetics were triggered by the position of the stage. Thus, light stimuli were timed to head position. Immediately prior to training, a test measurement was obtained

to gauge baseline VOR performance in the dark. After training, the VOR was re-tested. Mice were then held in their home cage during a recovery period (120 min; in darkness) and, afterward, returned to the apparatus so that the VOR could be retested to gauge retention of the learned response. Training sessions consisted of pairing optogenetic activity in association with the completion of ipsiversive or contraversive head movements or during the peak phase of ipsiversive head velocity. Measurements of VOR gain were also made in separate sessions that included training with the vestibular stimulus alone. This control condition measured for darkness-induced habituation. For each mouse, the order of training sessions was randomized with at least 48 hours between tests for all conditions. Baseline VOR performance across sessions was not significantly different (ANOVA with Bonferroni post hoc tests; $p > 0.05$).

Changes in VOR gain were computed as the percentage difference in VOR performance after training relative to the baseline measurement before training (ΔVOR). This normalization procedure facilitated comparison across sessions and between mice. To determine for learning-induced adaptation of the VOR with optogenetic pairing, baseline-normalized data were compared at time-matched points to control sessions of vestibular-only stimulation, thus disambiguating the influence of CF-evoked changes from that of darkness-induced habituation. For display, we also subsequently subtracted the darkness-induced change from measurements obtained in sessions with associative pairing of optogenetics and head motion; this made differences attributable to CF activity more apparent.

For visual-vestibular training, a high-contrast grating consisting of black and white vertical stripes was presented on the monitors using PsychoPy software. The grating was moved relative to the stage position either out-of-phase with the vestibular stimulus to produce a learned increase in VOR gain or in-phase with the vestibular stimulus resulting in a learned decrease in VOR gain. MLIs were photostimulated by laser pulses timed to the vestibular stimulus. Darkness-induced habituation was not a concern for this set of experiments because training occurred in the light provided by the visual stimulus. Session occurred in random order; differences in baseline VOR performance were not significant (ANOVA with Bonferroni post hoc tests; $p > 0.05$).

Fiber Photometry

Light from two different fiber-coupled LEDs (M405F1 and M470F3; Thorlabs) were launched into a fiber-compatible dichroic mirror mount (Fluorescence Mini-cube FMC6_E1[400-410]_F1[420-450]_E2[460-490]_F2[500-540]_O[570-650]_S; Doric Lenses). A 400 μm diameter patchcord (MFP_400/430/1100-0.48_FC-SMA, Doric Lenses) delivered excitation light to an implanted optical fiber (MFC_400/430-0.48_MF1.25_FLT, Doric Lenses) targeting the left flocculus. Light at these two different spectra (centered on λ = 405 and 470 nm) excited GCaMP6f producing either Ca^{2+}-insensitive (isosbestic) or Ca^{2+}-sensitive fluorescence emission, respectively (Kim et al., 2016). A time-division multiplexing scheme was used to alternate pulses of excitation light from the two LEDs (25 Hz). Excitation power from the two LEDs was set to produce similar levels of baseline fluorescence emission in both channels (~20 – 40 μW). Current controllers (LEDD1B; Thorlabs) triggered by TTLs were used to toggle the LEDs. Emitted fluorescence was collected through the same implanted optical fiber, passed back through the dichroic mirror mount, and detected using a femtowatt, visible wavelength photoreceiver (Model 2151; Newport) at a high sampling rate (2 kHz) with a DAQ board (PXIe-6363; National Instruments). Laser light from an amber DPSS laser (λ = 589 nm) was launched into the same dichroic mirror mount from a fiber port (PAF-X-11-A; Thorlabs). Prior to the fiber port, the laser light was gated by a fast shutter (NS15B1T0-ED; Vincent Associates) and modulated by an AOM (AA Opto-Electronic; MTS110-A3-VIS). The entire system was controlled using custom-written software in LabVIEW (National Instruments).

For analysis, fluorescence signals were de-multiplexed by assigning emission measurements to the corresponding excitation wavelength of light. Fluorescence signals collected during each light pulse were averaged, after dropping the first 15 samples to eliminate channel cross-talk. Thus, the effective rate of activity measurements was 25 Hz. When photoactivating CFs, the epochs containing the laser pulses were removed. In quiescent mice, laser stimuli were timed to the isosbestic measurements. This was not possible when CFs were stimulated during the VOR. Thus, for these experiments, isosbestic measurements were not obtained. This increased the effective frequency of Ca^{2+} activity measurements to 50 Hz in both control trials as well as photostimulus trials. For measurement of CF-evoked Ca^{2+} activity in quiescent mice, baseline fluorescence for calculating ΔF/F was simply mean fluorescence prior to the optogenetic stimulus. During VOR stimuli (trials lasted 120 s), baseline was defined as the dimmest 10%–25% of values in the entire distribution collected during the initial period of the record (4.8 s). This corresponds to the time periods between on-going, spontaneous events. Trials that included visual and optogenetic pairing (120 s) were presented in a randomized manner for each mouse with a period of separation (120 s) between each condition.

Histology and confocal imaging

For post hoc examination of transduced brain tissue, mice were anesthetized with a cocktail of ketamine and xylazine (100 mg/kg and 10 mg/kg, respectively) and then perfused transcardially with 0.1 M phosphate buffer (PB) followed by paraformaldehyde (PFA; 4% by volume in PB). The cerebellum and/or brainstem was isolated by dissection and subjected to post-fixation for ~12 hr (4°C) in the same PFA solution. Fixed tissue was then washed repeatedly with PB, embedded in 4% agar, and sliced into sections (100 μm) using a vibraslicer (VT1200S, Leica Biosystems). Slices were mounted on glass slides using anti-fade media (#S36963, Thermo Fisher Scientific). Fluorescence images were obtained from the mounted tissue using a Zeiss LSM 780 or LSM 880 confocal scanning microscope with excitation provided by argon and HeNe lasers. Maximum-intensity projection images were created from stacks of scanned tissue (Z-steps ~30 μm) using ZEN Light software (Zeiss).

We quantified CF transduction in IO injected mice using immunohistochemistry (IHC). For these experiments, C57BL/6J mice were bilaterally injected with AAV1-αCaMKII-eGFP in the IO. After several weeks, mice were perfused and the tissue collected and sectioned. Cerebellar slices from the floccular complex were incubated for one hour at room temperature in blocking solution (10% normal goat serum and 0.3% Titron X-100 in 1x TBS). Slices were then incubated overnight in primary antibodies at 4°C. We used a polyclonal rabbit anti-Calbindin D28-K (1:1,000, #CB38a, Swant) antibody to identify PCs. The antibody was diluted in 10% normal goat serum and 0.3% Triton X-100 in 1x TBS. In separate slices, mossy fibers were identified using a monoclonal mouse anti-VGLUT2 antibody (1:200, #ab579157, Abcam) diluted in 5% normal goat serum and 0.15% Triton X-100 in 1x TBS. Thereafter, slices were washed in 1x TBS and incubated for 1 hour at room temperature in secondary antibodies, either AlexaFluor 633 goat anti-rabbit (1:1,000 #A-21070, Thermo Fisher Scientific) or AlexaFluor 633 goat anti-mouse (1:200, #A-21072, Thermo Fisher Scientific) and then mounted on slides after repeated washes in PBS.

In IHC-labeled slices (n = 12 for each condition), GFP expression in CFs or mossy fibers was examined in tissue from the same cohort of mice (n = 4). The efficiency of CF transduction was quantified as the number of positively innervated PCs divided by the total number PCs (positively innervated PCs displayed clear GFP co-expression along their proximal dendrite in the molecular layer). To quantify mossy fiber transduction, VGLUT2-positive glomeruli were manually identified within the granule cell layer. Mossy fiber transduction was quantified as the number of co-labeled VGLUT2 and GFP glomeruli divided by the total number of VGLUT2-labeled terminals.

QUANTIFICATION AND STATISTICAL ANALYSIS

All population data are expressed as mean ± SEM and are indicated along with number of samples, in the figure or the figure legend. Differences were deemed significant with α values of $p < 0.05$ in paired or unpaired t tests. Where appropriate, group data were compared with 1 or 2-way ANOVA and significance between groups was determined with Bonferroni's, Tukey's, Dunnett's, or Dunn's multiple post hoc comparison tests.